


Full and unbiased solution of the Dyson-Schwinger equation in the functional integro-differential representation

Tobias Pfeffer and Lode Pollet

Department of Physics, Arnold Sommerfeld Center for Theoretical Physics, University of Munich, Theresienstrasse 37, 80333 Munich, Germany (Received 17 March 2018; revised manuscript received 11 October 2018; published 2 November 2018)

We provide a full and unbiased solution to the Dyson-Schwinger equation illustrated for ϕ^4 theory in 2D. It is based on an exact treatment of the functional derivative $\partial\Gamma/\partial G$ of the four-point vertex function Γ with respect to the two-point correlation function G within the framework of the homotopy analysis method (HAM) and the Monte Carlo sampling of rooted tree diagrams. The resulting series solution in deformations can be considered as an asymptotic series around $G = 0$ in a HAM control parameter c_0G , or even a convergent one up to the phase transition point if shifts in G can be performed (such as by summing up all ladder diagrams). These considerations are equally applicable to fermionic quantum field theories and offer a fresh approach to solving functional integro-differential equations beyond any truncation scheme.

DOI: [10.1103/PhysRevB.98.195104](https://doi.org/10.1103/PhysRevB.98.195104)

I. INTRODUCTION

Despite decades of research there continues to be a need for developing novel methods for strongly correlated systems. The standard Monte Carlo approaches [1–5] are convergent but suffer from a prohibitive sign problem, scaling exponentially in the system volume [6]. Diagrammatic Monte Carlo simulations [7–9] were developed to prevent this, scaling exponentially only in the expansion order [10]. However, this happens at the expense of substantially worse series convergence properties [11–13]. After nearly ten years and despite recent and tremendous progress [14–16], one may well fear that the combination of an asymptotic/divergent series and a mild sign problem is as prohibitive as the standard approaches. Recently [17], we therefore suggested to use the more flexible Dyson-Schwinger equation (DSE) instead of self-consistent Feynman diagrams [18] to provide a fully self-consistent scheme on the one and two particle level. Furthermore, we extended the homotopy analysis method (HAM) [19,20] to ϕ^4 field theory in two dimensions (2D) (providing us with more tools to enhance the convergence properties in a systematic way), and showed how the expansion in terms of rooted trees is amenable to a systematic Monte Carlo sampling. This expansion is furthermore convenient when dealing with multidimensional objects such as the four-point vertex function. Clearly, this is a radically different way at looking at interacting field theories. However, in our previous work [17], we truncated the DSE at the level of the six-point vertex. The infinite tower of equations for n -point correlation functions

was not solved and differences with the full, exact answer could be seen when the correlation length increases.

In this work, we solve the full DSE by writing them as a closed set of integro-differential equations. Within the HAM theory there exists a semianalytic way to treat the functional derivatives without resorting to an infinite expansion of the successive n -point correlation functions, cf. Refs. [21,22] where the DSE has been used to generate new weak coupling expansions. The unbiased numerical solution of the DSE is largely unexplored as it was considered to be too complex to be solved even in the simplest cases [23–25]. Furthermore, taking into account the functional derivatives deteriorates the convergence properties of the field theory substantially compared to the truncated case considered in Ref. [17]. Here we show how the remaining theory can be brought under control within the HAM as an asymptotic expansion of the HAM deformations in terms of an auxiliary convergence control parameter c_0 (times the two-point correlation function G) around $G = 0$, or even as a convergent expansion in the HAM deformations when a shift of G is possible, e.g., by solving the ladder equations. Although the ideas are illustrated for a 1d integral and ϕ^4 theory in 2D the convergence considerations and the methodology are generically applicable as long as the two-point and four-point correlation functions are bounded, and may just as well be applied to the better known Hedin [26] and parquet equations [27] or to the functional renormalization group equation [28,29].

The paper is organized as follows. The main ideas and results are introduced in Secs. II–IV. In Secs. II and III, we first analyze the toy model (i.e., the 1d integral, cf. Ref. [30]) to illustrate the approach and then proceed in Sec. IV with the full solution of the DSE for the ϕ^4 model in 2D. We provide further technical details, derivations, and information about the developed algorithm in Appendixes A–C. We do not include these details in the main text in order to provide the reader with a clear introduction to our new approach. The appendixes should be consulted in order to judge the validity

Published by the American Physical Society under the terms of the Creative Commons Attribution 4.0 International license. Further distribution of this work must maintain attribution to the author(s) and the published article's title, journal citation, and DOI.

and broad applicability of the results presented in the main text.

II. FUNCTIONAL CLOSURE

The functional closure is most easily demonstrated in the case of a 0D field theory. Consider the 1D integral

$$Z[J] = \int d\phi e^{-S[\phi]+J\phi} \text{ with } S[\phi] = \frac{1}{2}k\phi^2 + \frac{\lambda}{4!}\phi^4, \quad (1)$$

where $Z[J]$ is the generating functional of the n -point correlation functions $G^{(n)}$,

$$G^{(n)} = \frac{1}{Z[0]} \int d\phi e^{-S[\phi]}\phi^n = \frac{1}{Z[0]} \left. \frac{d^n Z[J]}{dJ^n} \right|_{J=0}. \quad (2)$$

Although in this example the generating functional $Z[J]$ is a real-valued function and the n -point correlation functions are real numbers, we will, nevertheless, use the terminology of (quantum) field theory (FT) as there will be no ambiguities. Moreover, we use the shorthand notation $G = G^{(2)}$ for the two-point correlation function. The DSE [31] can be derived by introducing an infinitesimal shift δ in the integration variable, $\phi \rightarrow \phi + \delta$, and expanding the resulting expression in powers of δ . This yields

$$\frac{dS}{d\phi} \left[\phi = \frac{d}{dJ} \right] Z[J] = JZ[J]. \quad (3)$$

The first derivative of the action S with respect to the field ϕ is promoted to a differential operator by the substitution $\phi = \frac{d}{dJ}$. The DSE (3) is a definition of the generating functional in terms of a differential equation equivalent to the definition of $Z[J]$ through (1). For a realistic FT (3) turns into a functional integro-differential equation, whereas (1) turns into a functional integral.

Instead of focusing on the solution of (1) we focus on (3). Differentiating (3) once with respect to J and setting $J = 0$ afterwards yields, after introducing the connected four-point correlation function $G_c^{(4)} = G^{(4)} - 3G^2$ and the four-point vertex function $\Gamma = -G^{-4}G_c^{(4)}$,

$$G^{-1} - k = \frac{\lambda}{2}G - \frac{\lambda}{6}G^3\Gamma. \quad (4)$$

This is the first equation in the expansion of the differential equation (3) into an infinite hierarchy of coupled equations for the correlation functions. We close the hierarchy by considering the generating functional to be a functional of the inverse noninteracting two-point correlation function k , $Z = Z[J = 0, k]$. Therefore we can write

$$G^{(4)} = -2\frac{dG}{dk} + G^2 \quad \text{and} \quad \Gamma = -2G^{-2}\frac{dG^{-1}}{dk} + 2G^{-2}. \quad (5)$$

We use (4) to expand the derivative of the inverse of the two-point correlation function with respect to k . This together with the chain rule

$$\frac{d\Gamma}{dk} = \frac{dG}{dk}\Gamma' = (G^4\Gamma - 2G^2)\Gamma', \quad (6)$$

where we denote the derivative with respect to G as Γ' , leads to the differential equation

$$\Gamma[G] = \lambda - \frac{3\lambda}{2}G^2\Gamma + \frac{\lambda}{2}G^4\Gamma^2 - \frac{\lambda}{3}G^3\Gamma' + \frac{\lambda}{6}G^5\Gamma'\Gamma. \quad (7)$$

A solution to (4) requires knowledge of the universal functional $\Gamma[G]$, which can be obtained by solving the differential equation (7). $\Gamma[G]$ is subsequently used in (4) and solved for G for a given inverse of the noninteracting two-point correlation function k . The combined system (4) and (7) is typically solved by a fixed point iteration. This gives the physical two-point correlation function G . The physical four-point vertex function Γ follows by evaluating the universal functional $\Gamma[G]$ for the physical G . In Ref. [17], we have already shown how to solve a realistic FT when only taking the first three terms on the right-hand side of (7) into account, i.e., working with a truncated version of $\Gamma[G]$, which has a finite convergence radius. Next, we examine the deterioration in convergence properties when taking the derivatives in (7) into account.

III. VERTEX EQUATION

The exact solution of (7) obtained by the implicit Euler method is shown in Fig. 1(a) for $\lambda = 10$. It agrees with inverting the functional $G[k] \rightarrow k[G]$ and plugging it into $\Gamma[k[G]]$. The additional vertical (horizontal) grid line corresponds to the physical $G(\Gamma)$ obtained for the model parameters $k = 1$, $\lambda = 10$. In case of a FT, (7) takes the form of a functional integro-differential equation and the implicit Euler method cannot be applied. It is therefore necessary to study semianalytic solutions to the differential equation (7).

The power series expansion $\Gamma[G] = \lambda + \lim_{M \rightarrow \infty} \sum_{n=1}^M c_n G^n$ has zero convergence radius [32]; bringing (7) into the form of $\Gamma'[G] = F[G, \Gamma[G]]$, we find that F is not holomorphic at $G = 0$, $\Gamma = \lambda$. An expansion around $G = 0$ corresponds to approaching the noninteracting limit by fixing λ and taking $k \rightarrow \infty$, i.e.,

$$Gk = \frac{1}{Z} \int d\phi \phi^2 e^{-\frac{1}{2}\phi^2 - \frac{\lambda}{4!k^2}\phi^4} \xrightarrow{k \rightarrow \infty} 1. \quad (8)$$

Further details about the analytic structure of the functional $\Gamma[G]$ are given in Appendix A. We observe numerically, see Fig. 1(b), that the power series solution to (7) has the properties of an asymptotic expansion, i.e., for every small G there exists an optimal truncation order M such that the truncated power series asymptotically approaches the exact answer with exponential accuracy. However, Fig. 1(a) shows that it is not possible to construct $\Gamma[G]$ as a power series at values of G where it corresponds to the physical G for the considered model parameters $k = 1$ and $\lambda = 10$.

A more powerful semianalytic method is the HAM [19]. The starting point is the construction of the homotopy

$$(1 - q)\mathcal{L}[\Phi[G, q] - u_{\Gamma,0}[G]] + qc_0\mathcal{N}[\Phi[G, q]] = 0 \quad (9)$$

for the differential equation (7). $\mathcal{N}[\Gamma[G]] = 0$ is the nonlinear differential operator defining (7) and \mathcal{L} is an arbitrary linear operator with the property $\mathcal{L}[0] = 0$. The homotopy (9) includes the deformation parameter $q \in [0, 1]$, which deforms the solution of \mathcal{L} from $\Phi[G, 0] = u_{\Gamma,0}[G]$ at $q = 0$ to the

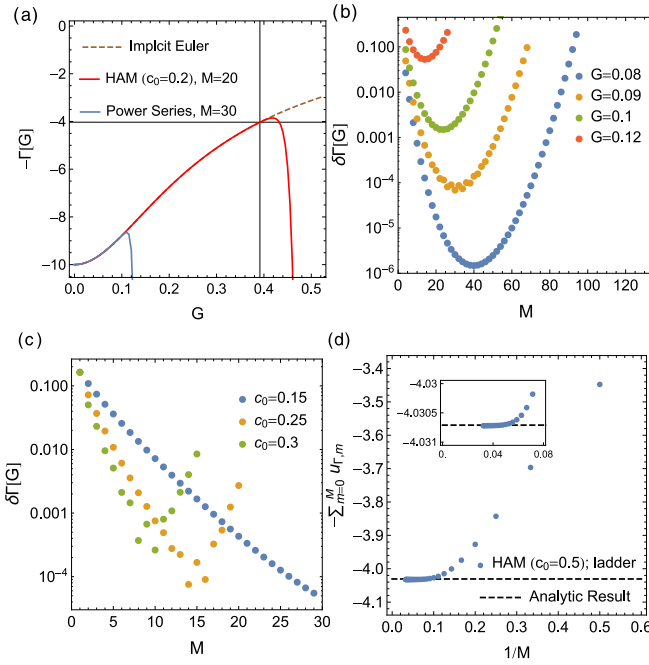


FIG. 1. (a) $\Gamma[G]$ at coupling $\lambda = 10$ obtained by the implicit Euler algorithm, a power series (asymptotic), and the HAM (asymptotic). The thin grid lines show the evaluation for the physical G, Γ for $k = 1$. (b) The relative error $\delta\Gamma[G]$ of a power series solution at small G shows the behavior of an asymptotic series in the maximal expansion order M . (c) The relative error $\delta\Gamma[G]$ of the HAM series solution around the noninteracting limit for $G = 0.3$ shows the behavior of an asymptotic series in the maximal deformation order M controlled by the convergence control parameter c_0 . (d) The convergence of the HAM series of deformations $u_{\Gamma,m}[G]$, $\sum_{m=0}^M u_{\Gamma,m}[G]$ with respect to a linear operator $\mathcal{L}_{\text{ladder}}[\Gamma[G]] = \Gamma[G] - \lambda + \frac{3\lambda}{2}G^2\Gamma[G]$, the ladder approximation to the vertex equation (7). The functional $\Gamma[G]$ is evaluated at the physical G for $k = 1$. The inset shows the convergence of the main plot on a much finer scale.

solution of the differential equation (7), $\Phi[G, 1] = \Gamma[G]$, at $q = 1$. $u_{\Gamma,0}[G]$ is the initial guess for the solution of $\mathcal{N}[\Gamma[G]] = 0$. The convergence control parameter c_0 controls the rate at which the deformation happens. The HAM attempts to find the solution of (9) through a Taylor series expansion in q , i.e., $\Phi[G, q] = u_{\Gamma,0}[G] + \sum_{m=1} u_{\Gamma,m}[G] q^m$. The expansion coefficients are given by $u_{\Gamma,m}[G] = \Phi^{(m)}[G, q = 0]/m!$ and can be obtained by the m th derivative of (9) with respect to q . Therefore the HAM gives a series solution of the differential equation (7) in terms of the deformation coefficients $u_{\Gamma,m}[G]$,

$$\Gamma[G] = u_{\Gamma,0}[G] + \sum_{m=1} u_{\Gamma,m}[G]. \quad (10)$$

We first use the easiest possible linear operator $\mathcal{L}[\Phi[G, q] - u_{\Gamma,0}[G]] = \Phi[G, q] - u_{\Gamma,0}[G]$. This choice can be straightforwardly generalized to functional integro-differential equations. In this case, the m th-order deformation in the HAM series solution is given in simple powers of G and additionally depend on the auxiliary parameter c_0 . Picking the identity operator, $\mathcal{L} = \text{id}$, is a too simplistic choice and does not

lead to a convergent HAM series solution. Nevertheless, the homotopy introduces the convergence parameter c_0 which gives us additional freedom since the effective parameter $c_0 G$ can always be made small as long as G remains finite and therefore the limitations of the standard power series approach can be overcome. As is illustrated in Figs. 1(a) and 1(c), the asymptotic nature can then be postponed to larger expansion orders for smaller c_0 but with larger deviations from the exact result at low expansion orders. This approach can be generalized to realistic field theories in which case $c_0 \|G\|$ can be chosen to be small where $\|G\|$ denotes the L^p norm of the two-point correlation function. In the next section, we show numerically that this holds for a generic FT and that it is possible to get accurate results even close to a second-order phase transition at which $\|G\|$ gets unbounded.

Before extending this approach to a realistic FT we like to emphasise the great potential and novelty of the Dyson-Schwinger and homotopy approach to FT. Instead of constructing the HAM series expansion around the noninteracting limit, $G = 0$, we can use the linear operator $\mathcal{L} = \mathcal{L}_{\text{ladder}}$ to construct a homotopy with respect to the analytically solvable ladder approximation, $\mathcal{L}_{\text{ladder}}[\Gamma[G]] = \Gamma[G] - \lambda + \frac{3\lambda}{2}G^2\Gamma[G]$. In an FT, the term $\frac{3\lambda}{2}G^2\Gamma[G]$ sums up all RPA-ladder diagrams. The resulting homotopy can be written as

$$\begin{aligned} \Gamma_q[G] &= \lambda - \frac{3\lambda}{2}G^2\Gamma_q + \frac{\tilde{\lambda}(q, c_0)}{2}G^4\Gamma_q^2 \\ &\quad - \frac{\tilde{\lambda}(q, c_0)}{3}G^3\Gamma_q' + \frac{\tilde{\lambda}(q, c_0)}{6}G^5\Gamma_q'\Gamma_q, \end{aligned} \quad (11)$$

where $\tilde{\lambda}(q, c_0) = \frac{c_0 q}{1 - q + c_0 q} \lambda$,

which should be compared to the closed DSE (7). Taking into account the equivalence between the functional integral and the functional integro-differential approach, an important question is if (11) can be related back to an auxiliary action such as $S = S_0(q) + q S_{\text{int}}$, which has been considered in variational perturbation theory approaches [33,34] or shifted action approaches [35]. $S_0(q)$ is some quadratic auxiliary action and S_{int} is the interaction part such that $S(q = 1) = S$ with S the physical action of the theory under consideration. A general feature of DSEs is that each term on the right-hand side of (7) contributes exactly with one factor of the bare coupling constant. In contrary, for the homotopy (11), there are terms contributing with a modified bare coupling constant $\tilde{\lambda}$ and therefore (11) can not be associated with the closed DSE of an auxiliary action. In conclusion, we see that the HAM series solution is effectively an expansion with respect to the truncated interacting ladder model which has no correspondence in a functional integral representation and can only be written down in the equations of motion approach. Figure 1(d) shows that the HAM series with respect to the ladder approximation yields a convergent series solution. Moreover, we find that the HAM series solution is globally convergent, i.e., it is not restricted by a finite, c_0 -dependent convergence interval. Therefore we also find a convergent solution for values of G , which correspond to $G[k]$ with $k < 0$. In this parameter regime, the action (1) has degenerate minima and the standard perturbative series for the vertex

function is not Boreal summable [36]. For further details see Appendix A.

IV. ϕ^4 THEORY IN 2D

Consider the \mathbb{Z}_2 -symmetric ϕ^4 theory on a 2D lattice with action

$$S[\phi] = \frac{1}{2} \sum_{i,j} \phi_i G_{0;i,j}^{-1} \phi_j + \frac{\lambda}{4!} \sum \phi_i^4. \quad (12)$$

The inverse noninteracting two-point correlation function is given by $G_{0;i,j}^{-1} = -\square_{i,j} + m^2 \delta_{i,j}$, where $\square_{i,j}$ denotes the discretized Laplace operator in 2D. For $m^2 < 0$, this model undergoes a second order phase transition from a magnetically ordered to an unordered phase at a critical coupling constant $\lambda_c(m^2)$. The phase transition is signalled by the divergence of the magnetic susceptibility $\chi = G(p=0)$, which leads to the same critical exponents as for the 2D Ising model previously studied diagrammatically with grassmannization techniques [37]. In our simulation, we use $m^2 = -0.5$, which corresponds to $\lambda_c(m^2) \sim 2$. The coupled set of equations for (12), generalization of (4) and (7) and derived in Appendix B, are graphically depicted in Fig. 2.

We use an extension of the Monte Carlo algorithm developed in Ref. [17] to sample the expansion of the HAM in rooted tree diagrams. The detailed algorithm, especially the correct implementation of the functional derivatives, is discussed in Appendix C. Figure 3 shows the result for the divergence of the susceptibility χ for successive approximations of $\Gamma[G]$ and for the full solution of the functional integro-differential equation. It should be pointed out that the coupled

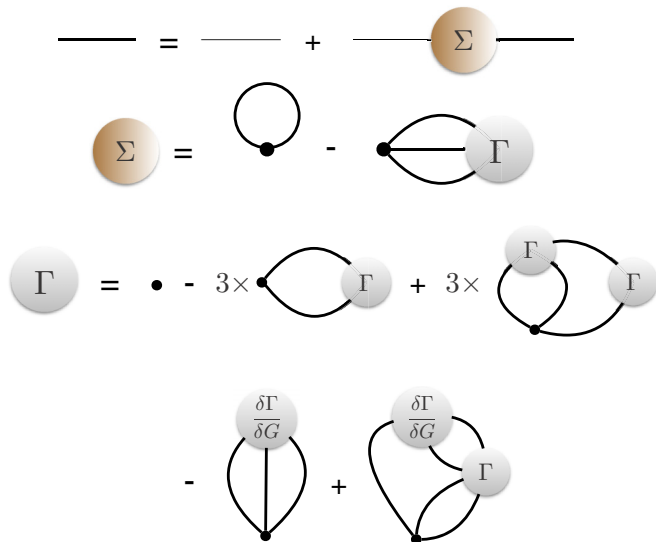


FIG. 2. The coupled set of equations defining model (12) is closed through a functional integro-differential equation. Each diagram is in one-to-one correspondence with the terms in (4) and (7). The noninteracting two-point correlation function $G_{0;i,j}$ is denoted by a thin line, the two-point correlation function $G_{i,j}$ by a bold line, and the bare vertex by a dot. The correct convolution of lattice indices can be obtained by standard diagrammatic rules. The terms without functional derivatives involve the permutation of external indices and is denoted by the factor 3.

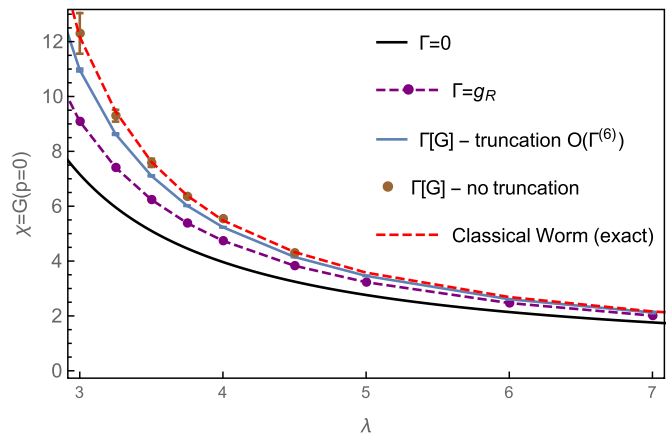


FIG. 3. The development of the divergence of the susceptibility $\chi = G(p=0)$ close to the phase transition for the model (12). Various approximations of the universal functional $\Gamma[G]$ yield systematic, quantitative errors whereas the full solution captures the correct quantitative behavior. The black, dashed purple and blue lines were obtained in Ref. [17] and correspond to different truncations of the functional $\Gamma[G]$. The black approximation corresponds to $\Gamma[G] = 0$, the dashed purple line to $\Gamma[G] = g_R = \lambda(1 + 3\lambda/2 \int_p G(p)^2)^{-1}$ and the blue line to the truncation of $\Gamma[G]$, which takes into account only the first three diagram elements on the right-hand side of Fig. 2 in the functional integro-differential equation for $\Gamma[G]$, i.e., corrections of the order of the six-point vertex function $\Gamma^{(6)}$ are neglected.

set of equations, Fig. 2, are defining the FT (12) directly in the thermodynamic limit, i.e., results obtained by our method are for infinite system sizes. The results are compared to the numerically exact simulation of model (12) with the classical Worm algorithm [38] on system sizes which are much larger than the correlation length. We find that it is possible to obtain controlled results with our current Monte Carlo algorithm up to $\chi \sim 10$, which corresponds to a correlation length of $\xi \sim 3$. Our diagrammatic Monte Carlo sampling is based on a direct sampling of all topologies of rooted tree diagrams at a given order. This naive approach leads to sampling problems at higher deformation orders and restricts the order to 5–6. Due to the sign alternation between the linear and quadratic terms in the vertex equation the sampling suffers from a sign problem discussed in Ref. [17] for the case of the stochastic construction of a truncated functional. We find no qualitative difference if the functional derivative terms are added. We performed extensive Monte Carlo simulations such that the error bars are exclusively determined by the extrapolation of the lowest deformation orders as is shown in Fig. 4. It is only possible to extrapolate the inverse of the two-point correlation function and therefore the error introduced through the extrapolation is growing rapidly as the susceptibility diverges, cf. Fig. 3. It should be pointed out that we have no global excess to $\Gamma[G]$ but only to a stochastic, local evaluation of the universal functional through the diagrammatic Monte Carlo sampling of the HAM series solution in terms of rooted tree diagrams. Further details about the algorithm are presented in Appendix C. In order to obtain the results in Fig. 3 through this evaluation of $\Gamma[G]$, we simplified the calculation by starting the fixed point iteration for the coupled

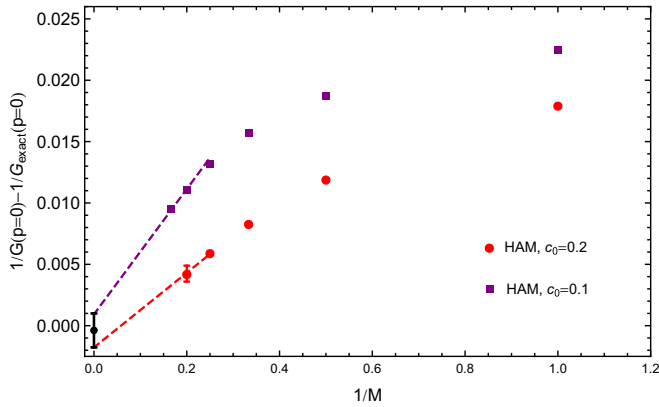


FIG. 4. In order to obtain an error estimate for the extrapolation of the homotopy series we use a linear extrapolation for different deformation parameters c_0 . We make sure within error bars that results extrapolate to the same value for different c_0 . The plot shows the results for $\lambda = 3.5$ where the correlation length is already large enough such that there are considerable deviation from the exact result if only a truncated functional $\Gamma[G]$ has been considered, cf. Fig. 3.

system in Fig. 2 at the numerically exact two-point correlation function. This reduces the computational time as we have to perform only a single fixed point iteration step. For more general starting points of the fixed point iteration we refer to Ref. [17]. Figures 3 and 4 show that, although there is no single physical small parameter close to the phase transition, we obtain controlled results as we can construct the homotopy (9) always with respect to a small enough c_0 . In the vicinity of the second-order phase transition, $\|G\| \rightarrow \infty$ implies that $c_0 \rightarrow 0$ but in order to get meaningful results, the number of required deformations increases rapidly. Therefore, due to the limited number of deformations, which can be computed with our algorithm, we can not go closer to the phase transition. For transitions where $\|G\|$ remains finite (the divergence may then occur in the four-point vertex function), this argument is not applicable.

V. OUTLOOK

Although the approach to FT introduced in this work is illustrated for the simple though representative case of ϕ^4 theory, models with arbitrary two-body interactions in its symmetric phase can be tackled on the same footing. As shown in Appendix B, the transition from the functional integral representation for general models to functional integro-differential equations yields exactly the same set of equations as depicted in Fig. 2. The only difference is that the convolution of indices in the diagrams representing the functional integro-differential equation is with respect to a collective index i , which summarizes all possible field labels of the considered model. The statistics of fermionic fields translate into additional signs for the permutations of external indices in the diagrams of Fig. 2 and into sign alternating two-point correlation functions.

VI. CONCLUSION

In conclusion, we have introduced a general approach to tackle FT through full and unbiased solutions of

functional integro-differential equations derived from the DSE. We showed for a toy model that by using the semi-analytic HAM we can solve the differential equation for the vertex function. The HAM gives a convergent series solution if the homotopy is constructed with respect to the analytically solvable ladder approximation for the four-point vertex function or an asymptotic series solution, which can be controlled by the convergence control parameter c_0 if the homotopy is constructed around the noninteracting limit. The latter result found for the toy model can be readily applied to a simple FT where the asymptotic series solution can be controlled by the convergence control parameter c_0 even close to a second-order phase transition.

The open data for this project can be found at Ref. [39].

ACKNOWLEDGMENTS

The authors would like to thank D. Hügel, A. Toschi and the participants of the *Diagrammatic Monte Carlo Workshop* held at the Flatiron Institute, June 2017 for fruitful discussions and valuable input. This work is supported by FP7/ERC Consolidator Grant No. 771891, and the Nanosystems Initiative Munich (NIM).

APPENDIX A: ANALYTIC STRUCTURE OF THE UNIVERSAL FUNCTIONAL $\Gamma[G]$: CONVERGENT HAM SERIES SOLUTION

In order to obtain the analytic structure of $\Gamma[G]$ near $G = 0$, we first consider the analytic solution to the integral

$$Z = \int d\phi e^{-S[\phi]} \text{ with } S[\phi] = \frac{1}{2}k\phi^2 + \frac{\lambda}{4!}\phi^4. \quad (\text{A1})$$

The analytic solution to this integral for $k \in \mathbb{C}$ with fixed $\lambda \in \mathbb{R}^+$ is given as

$$Z[k] = e^{\frac{3k^2}{4\lambda}} \begin{cases} \sqrt{3}\sqrt{\frac{k}{\lambda}} K_{\frac{1}{4}}\left(\frac{3k^2}{4\lambda}\right) & \text{Re}(k) > 0 \\ \sqrt{\frac{3}{2}}\pi\sqrt{-\frac{k}{\lambda}} \left(I_{\frac{1}{4}}\left(\frac{3k^2}{4\lambda}\right) + I_{-\frac{1}{4}}\left(\frac{3k^2}{4\lambda}\right) \right) & \text{Re}(k) < 0 \end{cases}. \quad (\text{A2})$$

Here, $I_n(z)/K_n(z)$ are the modified Bessel functions of the first/second kind and $Z[k=0] = (3/2\lambda)^{1/4}\Gamma(1/4)$ where $\Gamma(x)$ is the Gamma function. The integral (A1) can be regarded as an integral representation of the function Z defined in (A2). The same holds for the two-point correlation function $G[k]$, which we do not show here. The important point is that both $Z[k]$ and $G[k]$ are piecewise-defined functions in k , which can be represented by a single integral expression. There exists also a differential equation equivalent to the integral representation of the function $Z[k]$ or $G[k]$. For $G[k]$, this is the coupled system of differential equations:

$$\begin{aligned} G_{\pm}[k]^{-1} - k &= \frac{\lambda}{2}G_{\pm}[k] - \frac{\lambda}{6}G_{\pm}[k]^3\Gamma_{\pm}^{(4)}[k], \\ \Gamma_{\pm}[k] &= \lambda - \frac{3\lambda}{2}G_{\pm}[k]^2\Gamma_{\pm}[k] + \frac{\lambda}{2}G[k]_{\pm}^4[\Gamma_{\pm}^{(4)}]^2 \\ &\quad + \frac{\lambda}{6}G_{\pm}[k]\frac{d\Gamma_{\pm}^{(4)}}{dk}. \end{aligned} \quad (\text{A3})$$

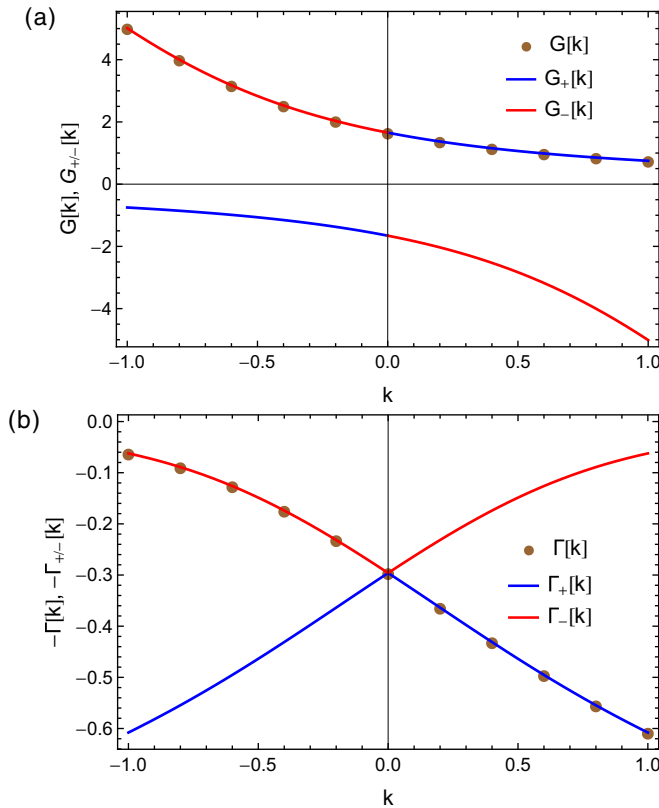


FIG. 5. The two solutions for $G(\Gamma)_{\pm}[k]$ of (A3) on the real axis for $\lambda = 1$. The physical solution $G(\Gamma)[k]$ corresponds to the solution $G(\Gamma)_{+}[k]$ for $k > 0$ and $G(\Gamma)_{-}[k]$ for $k < 0$, cf. (A2).

There are two independent solutions to this equation for G and, consequently, also for Γ denoted as $G_{\pm}[k]$ and $\Gamma_{\pm}[k]$, respectively. While (A1) is single-valued, the solution to the system of equations (A3) in principle leads to two independent solutions. They are shown for $G_{\pm}[k]$, $\Gamma_{\pm}[k]$ on the real axis in Fig. 5. We will show in the following that the analytic structure of $\Gamma[G]$ near $G = 0$ can be understood from the existence of the two independent solutions to (A3). Formally, $\Gamma[G]$ can be obtained from $\Gamma_{\pm}[k]$ by inverting the relation $G = G_{\pm}[k]$. There are two independent solutions which for some k satisfy $G = G_{+}[k_1] = G_{-}[k_2]$. This leads to two branches for $\Gamma[G]$ where $\Gamma[G]$ must evaluate to $\Gamma_{+}^{(4)}[k_1]$ on the first branch and to $\Gamma_{-}^{(4)}[k_2]$ on the second branch. In order to obtain the analytic structure of $\Gamma[G]$ near $|G| = 0$, it is necessary to study the intersection of the images of G_{\pm} for elements which satisfy $|G| \rightarrow 0$. The complete circle in the complex G plane $|G|e^{i\phi}$, $\phi \in [0, 2\pi]$ for $|G| \rightarrow 0$ in Fig. 6 is included in the image of $G_{+}[k]$ and can be obtained by the parametrization $k = |k|e^{-i\phi}$ where $|k| \rightarrow \infty$. On the other hand, the image of $G_{-}[k]$ includes two segments of the circle $|G|e^{i\phi}$, namely, with $\phi \in [\frac{\pi}{4}, \frac{3\pi}{4}]$ and $\phi \in [\frac{5\pi}{4}, \frac{7\pi}{4}]$ and can also be obtained by the parametrization $k = |k|e^{-i\phi}$. Therefore there are branch cuts starting from $G = 0$ cutting the complex G plane in the $\pm\frac{\pi}{4}$ direction.

According to the above result a power series solution around $\tilde{G} \in \mathbb{R}^{+}$, should have convergence radius $R = \sin(\frac{\pi}{4})\tilde{G}$. The convergence radius can also be determined

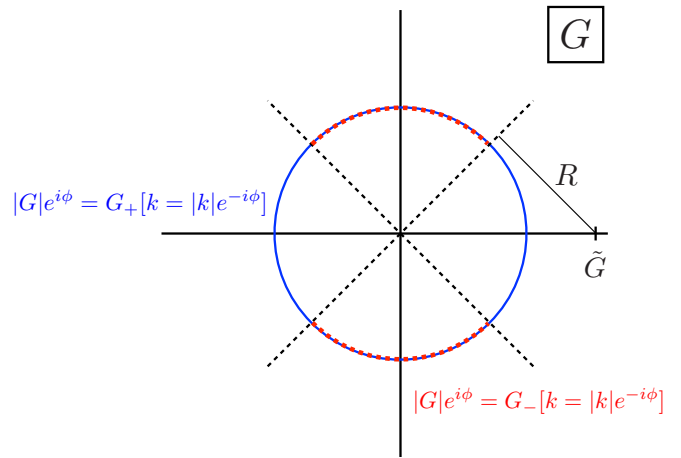


FIG. 6. The elements of the images of $G_{\pm}[k]$ onto the circle $|G|e^{i\phi}$ for $|G| \rightarrow 0$. For $\phi \in [\frac{\pi}{4}, \frac{3\pi}{4}]$ and $[\frac{5\pi}{4}, \frac{7\pi}{4}]$, G_{\pm} map onto the same G . Therefore $\Gamma[G]$ has to be single valued on $\phi \in [-\frac{\pi}{4}, \frac{\pi}{4}]$ and $[\frac{3\pi}{4}, \frac{5\pi}{4}]$ and multivalued on $\phi \in [\frac{\pi}{4}, \frac{3\pi}{4}]$ and $[\frac{5\pi}{4}, \frac{7\pi}{4}]$. The Taylor series of $\Gamma[G]$ around $\tilde{G} \in \mathbb{R}^{+}$ has the convergence radius $R = \sin(\frac{\pi}{4})\tilde{G}$.

numerically by considering the coefficients c_n in the power series $\Gamma[G] = \sum_n c_n (G - \tilde{G})^n$. The power series can be obtained by using the analytically known result for $\Gamma_{+}^{(4)}[G_{+}[k]]$ on the real axis, i.e., $c_0 = \Gamma[\tilde{G}]$. As shown in Fig. 7, the numerically obtained convergence radius from the large order behavior of the coefficients c_n agrees with the expected convergence radius.

Moreover, we numerically find a convergent HAM series solution if we are considering a linear operator \mathcal{L} such that the HAM does not yield a series solution around the noninteracting limit $G = 0$. With the simple choice $\mathcal{L}_{\text{ladder}}[\Gamma[G]] = \Gamma[G] - \lambda + \frac{3\lambda}{2}G^2\Gamma[G]$ we obtain the result shown in Fig. 8(a). The linear operator is the ladder approximation to the functional $\Gamma[G]$ and for a field theory

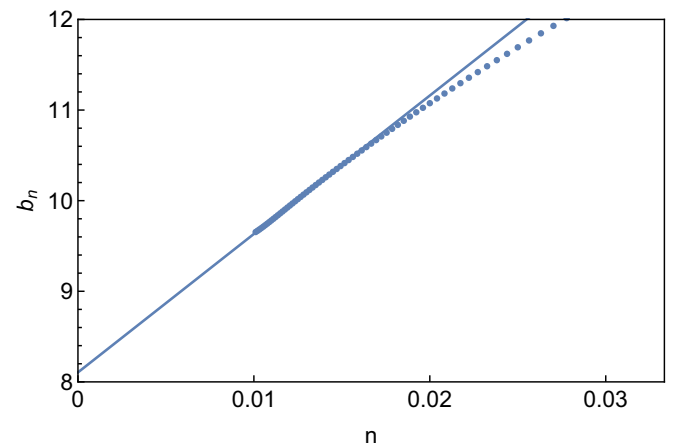


FIG. 7. The linear extrapolation of the large order asymptotic $b_n^2 = \frac{c_{n+1}c_{n-1} - c_n^2}{c_n c_{n-2} - c_{n-1}^2}$ yields a convergence radius $R \approx \frac{1}{8.105} = 0.123$, which can be compared to the expected convergence radius of $R = \sin(\frac{\pi}{4})0.172 = 0.122$. Here, $\tilde{G} = G_{+}[k = 5] = 0.172$ has been considered.

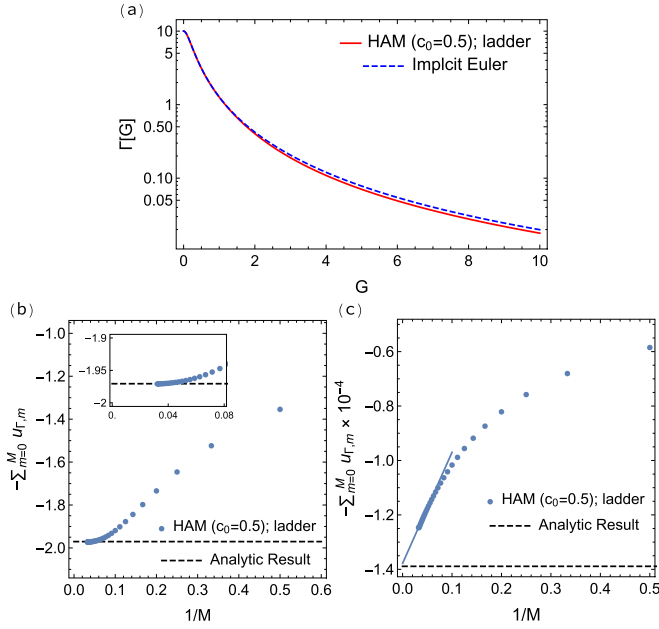


FIG. 8. (a) The approximation to the HAM series solution $\Gamma[G] = \lim_{m \rightarrow \infty} \sum_{m=0}^M u_{\Gamma,m}$ with $M = 30$ on a semilogarithmic scale. The HAM series converges globally, i.e., it is not limited to a finite, c_0 -dependent convergence interval. Therefore convergence can be achieved for large values of G which corresponds to $k < 0$. The truncation of the series solution at $M = 30$ already gives decent results for large G without extrapolating the series solution. The convergence of the HAM series solution is explicitly demonstrated in (b) and (c). Without tuning the convergence control parameter c_0 , convergence can be observed both for small (b) $G[k = -1] \approx 0.73$ and large (c) $G[k = -200] \approx 12$ G .

sums up all RPA-ladder diagrams. Therefore the HAM series solution is an expansion with respect to the interacting ladder approximation. With the linear operator $\mathcal{L}_{\text{ladder}}$ the HAM series solution gives a globally convergent solution. Therefore the series also converges for large values of G . This regime corresponds to the double well potential, i.e., $k < 0$. The convergence is demonstrated in Figs. 8(b) and 8(c). The HAM series solution is converging for arbitrary G without tuning the convergence control parameter c_0 .

APPENDIX B: FUNCTIONAL CLOSURE FOR FIELD THEORY

In this appendix, we derive a closed system of functional integro-differential equations for general interacting many-body models with arbitrary two-body interaction. These equations define the many-body theory under consideration in a functional integro-differential formulation.

1. Correlation functions and functional derivatives

To find a closed set of equations for correlation functions we write high-order correlation functions as functional derivatives of low order correlation functions. In this section, we show how we define the functional derivatives in a collective index notation.

In Sec. II, the algebraic 0D quantum field theory (FT)

$$Z[J] = \int d\phi e^{-S[\phi]+J\phi} \quad \text{with} \quad S[\phi] = \frac{1}{2}k\phi^2 + \frac{\lambda}{4!}\phi^4 \quad (\text{B1})$$

was considered, where $Z[J]$ is the generating functional of the n -point correlation functions

$$G^{(n)} = \frac{1}{Z[0]} \int d\phi e^{-S[\phi]} \phi^n = \frac{1}{Z[0]} \left. \frac{d^n Z[J]}{dJ^n} \right|_{J=0}. \quad (\text{B2})$$

We extend the definition of the generating functional $Z[J]$ with a one-point source term J to a two-point source term. The inverse noninteracting two-point correlation function k can be thought of as a two-point source term. Therefore the partition function $Z = Z[J = 0]$ is considered to be a generating functional with respect to k , $Z = Z[k]$. The two-point correlation function $G = G^{(2)}$ can be obtained by differentiation with respect to the two-point source term k ,

$$G = -2 \left. \frac{d \ln Z[k]}{dk} \right|_{k_{\text{phys}}}. \quad (\text{B3})$$

In order to practically use (B3), $Z[k]$ has to be computed for arbitrary $k \in \mathbb{R}$ and afterwards the derivative has to be evaluated at $k = k_{\text{phys}}$.

We first discuss the extension to a FT for the prototypical \mathbb{Z}_2 symmetric ϕ^4 model on a lattice in arbitrary dimensions D ,

$$Z[J] = \int d(\phi) e^{-S[\phi] + \sum_i J_i \phi_i} \quad \text{with} \quad S[\phi] = \frac{1}{2} \sum_{i,j} \phi_i G_{0,i,j}^{-1} \phi_j + \frac{\lambda}{4!} \sum_i \phi_i^4. \quad (\text{B4})$$

In this case, $G_0^{-1} \in \mathbb{R}^{L \times L}$ with L the number of lattice sites and $G_{0,i,j}^{-1} = G_{0,i,j;\text{phys}}^{-1} = -\square_{i,j} + m^2 \delta_{i,j}$, where \square is the discretized Laplace operator in D dimensions. The measure of the functional integral is denoted by $d(\phi)$. The n -point correlation function carries now additional lattice indices and is defined as

$$G_{i_1, \dots, i_n}^{(n)} = \langle \phi_{i_1} \dots \phi_{i_n} \rangle = \frac{1}{Z[0]} \int d(\phi) e^{-S[\phi]} \phi_{i_1} \dots \phi_{i_n}. \quad (\text{B5})$$

In analogy with the 0D case, we consider $Z = Z[J = 0] = Z[G_0^{-1}]$ and write the two-point correlation function as

$$G_{i,j} = -2 \left. \frac{\delta \ln Z[G_0^{-1}]}{\delta G_{0,i,j}^{-1}} \right|_{G_{0,\text{phys}}^{-1}}. \quad (\text{B6})$$

Therefore $Z[G_0^{-1}]$ has to be computed for arbitrary $G_0^{-1} \in \mathbb{R}^{L \times L}$ and only after the derivative has been taken the expression is evaluated in the subspace of physical $G_0^{-1} = G_{0,i,j;\text{phys}}^{-1}$.

In particular, although $G_{0,i,j;\text{phys}}^{-1}$ lies inside the subspace of translational invariant G_0^{-1} the calculation of $Z[G_0^{-1}]$ must not be restricted to this physical subspace. Translational invariance can only be restored after the functional derivative of $Z[G_0^{-1}]$ is evaluated at $G_{0,\text{phys}}^{-1}$.

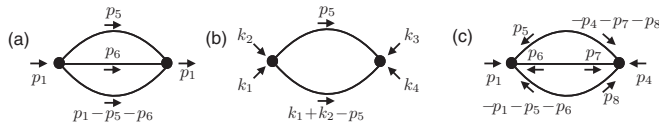


FIG. 9. Feynman diagrams in momentum space contributing to different correlation functions for ϕ^4 theory with action (B4). The lines represent noninteracting two-point correlation functions G_0 whereas the interaction vertex is represented by the dot. Due to the local interaction, momentum is conserved at each vertex. (a) The second-order contribution to the self-energy. Due to the translational symmetry of the ϕ^4 model incoming and outgoing momenta have to be equal and G_0 depends only on a single momentum variable. (b) A second-order contribution to the four-point vertex function depending on the four external momentum variables k_i . Due to translational symmetry, $\delta(k_1 + k_2 + k_3 + k_4)$, the four-point vertex function effectively depends on three momentum variables. (c) The second-order diagram contributing to the self-energy without assuming translational symmetry. Therefore incoming and outgoing momenta do not have to be equal and the two-point correlation function lines depend on two momentum variables.

The following argument [40] illustrates that this is indeed indispensable. The four-point correlation function $G_{i_1, i_2, i_3, i_4}^{(4)} = \langle \phi_{i_1} \phi_{i_2} \phi_{i_3} \phi_{i_4} \rangle$ can be written as

$$G_{i_1, i_2, i_3, i_4}^{(4)} = -2 \left. \frac{\delta G_{i_1, i_2}}{\delta G_{0; i_3, i_4}^{-1}} \right|_{G_{0; \text{phys}}^{-1}} + G_{i_1, i_2} G_{i_3, i_4}. \quad (\text{B7})$$

Model (B4) is translational invariant and therefore $G^{(4)}$ depends on three relative distances, e.g., $i_1 - i_2$, $i_1 - i_3$, $i_1 - i_4$. If translational invariance is already restored before taking the functional derivative in (B7), i.e., taking the functional derivative only in the restricted subspace of translational invariant G_0^{-1} , the right-hand side depends only on two relative distances $i_1 - i_2$, $i_3 - i_4$. In this case, the functional derivative does not provide the full information about all values of the four-point correlation function. This shows that it is crucial to consider $G_0^{-1} \in \mathbb{R}^{L \times L}$ and not perform the calculation in a restricted subspace. We can also consider an argument based on diagrammatic reasonings which is closer to the actual computational techniques introduced in this chapter. The above result can be obtained by taking into account the following considerations. Formally, a FT can also be defined through its series expansion of correlation functions in terms of Feynman diagrams. The functional derivative with respect to G_0 (related to the one with respect to G_0^{-1} through the chain rule of functional differentiation) can be considered for each diagram. The action of this derivative on a single Feynman diagram is diagrammatically represented by removing one G_0 line in all possible ways. The result of cutting a single G_0 line is a new diagram with two additional external legs, which can be a Feynman diagram in the series expansion of a higher order correlation function. The precise relation will be derived in the following chapter. We consider this process for a specific example where translational invariance is already restored before taking the functional derivative. The functional derivative of the diagram in Fig. 9(a) in momentum

space will give the following expression:

$$\begin{aligned} & \frac{1}{3} \frac{\delta}{\delta G_0(p_3)} \int_{p_5, p_6} G_0(p_1 - p_5 - p_6) G_0(p_5) G_0(p_6) \\ &= \int_{p_5} G_0(p_1 - p_3 - p_5) G_0(p_5). \end{aligned} \quad (\text{B8})$$

Due to translational invariance G_0 is diagonal in momentum space and depends only on a single momentum variable. The resulting diagram obtained from this functional differentiation is depicted in Fig. 9(b). It contributes to the Feynman diagrammatic expansion of the four-point vertex function. However, as we already assumed translational invariance before taking the derivative we can obtain information only in the subspace $k_1 = -k_4 = p_1$ and $k_2 = -k_3 = -p_3$.

The contribution for arbitrary external momentum variables is given by the functional derivative of the diagram in Fig. 9(c). Translational invariance is not taken into account yet and therefore G_0 depends on two momentum variables. In this case, differentiating the diagram gives

$$\begin{aligned} & \frac{1}{3} \frac{\delta}{\delta G_0(p_2, p_3)} \int_{p_5, p_6, p_7, p_8} G_0(p_5, -p_4 - p_7 - p_8) G_0(p_6, p_7) \\ & \times G_0(-p_1 - p_5 - p_6, p_8) \Big|_{G_0 = G_{0, \text{phys}}} \\ &= \delta(p_1 + p_2 + p_3 + p_4) \int_{p_5} G_0(p_1 + p_2 - p_5) G_0(p_5), \end{aligned} \quad (\text{B9})$$

which is exactly the analytic expression for Fig. 9(b) with $k_i = p_i$.

This result can be generalized to more complicated symmetries such as interacting fermions with spin σ on a lattice with a translational invariant hopping matrix h and local on-site Hubbard type interaction. The free part S_0 of the action $S = S_0 + S_{\text{int}}$ can then be written as

$$S_0[\bar{\psi}, \psi] = \int_0^\beta d\tau d\tau' \sum_{\sigma, \sigma'; i, j} \bar{\psi}_{i, \sigma}(\tau) G_{0; i, j, \sigma, \sigma'}^{-1, \bar{\psi} \psi}(\tau, \tau') \psi_{j, \sigma'}(\tau'), \quad (\text{B10})$$

where $G_{0; i, j, \sigma, \sigma'}^{-1, \bar{\psi} \psi}(\tau, \tau') = G_{0; i, j, \sigma, \sigma'; \text{phys}}^{-1}(\tau, \tau') = \delta_{\sigma, \sigma'} \delta(\tau - \tau') [(\partial_\tau - \mu) \delta_{i, j} + h_{i, j}]$ and the interacting part S_{int} describes a local interaction, which does not break U(1) symmetry nor SU(2) spin symmetry nor does it violate translational invariance in space and imaginary time.

We focus in the following on the U(1) symmetry leading to particle number conservation but note that exactly the same argument can be used for SU(2) spin symmetry.

A second-order diagram contributing to the self-energy for this model is given in Fig. 10(a). We only consider the labels of the diagram due to the U(1) symmetry where incoming lines denote ψ and outgoing lines denote $\bar{\psi}$. Due to the U(1) symmetry particle number is conserved and the number of ingoing lines equals the number of outgoing lines. Taking the derivative of this diagram with respect to $G_0^{\bar{\psi} \psi}$ we obtain the diagram in Fig. 10(b), which contributes to the four-point correlation function. The diagram in Fig. 10(a) is not the only diagram which upon cutting a single propagator line leads to the diagram in Fig. 10(b). If we allow for U(1) symmetry

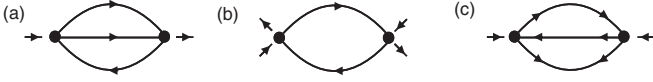


FIG. 10. Feynman diagrams for the fermionic model with free action (B10) and Hubbard type interactions. The lines represent noninteracting two-point correlation functions G_0 , whereas the interaction vertex is represented by the dot. The diagrams are only labeled by the arrows on the lines which corresponds to U(1) symmetry. Further labels are suppressed. Incoming lines represent $\bar{\psi}$ fields and outgoing lines represent ψ fields. As the Hubbard type density-density interaction preserves U(1) symmetry the number of ingoing and the number of outgoing lines on each vertex have to be equal. (a) The second-order diagram contributing to the diagonal part of the self-energy. The number of incoming and outgoing lines are equal and therefore the diagram contributes to the diagonal component of the self energy. (b) A second-order diagram contributing to the four-point vertex function. (c) The second-order diagram contributing to the off-diagonal part of the self-energy. There are two incoming lines but no outgoing lines therefore the diagram contributes only in the case of broken U(1) symmetry.

breaking we can also consider the diagram in Fig. 10(c), which contributes to the off-diagonal part of the self-energy. The particle number is not conserved for this diagram as there are two incoming lines but no outgoing lines. The diagram includes a off-diagonal G_0 line, $G_0^{\bar{\psi}\psi}$, which is indicated by two arrows on that line pointing in different directions. Cutting this G_0 line also leads to the diagram in Fig. 10(b), which preserves particle number conservation. This example shows, in analogy with translational invariance, that in an intermediate stage of the calculation U(1) symmetry can be broken and only after the derivative has been taken all symmetries of the action have to be respected.

Concluding, we showed that in general G_0^{-1} has to be defined outside the subspace of physical inverse noninteracting two-point correlation functions. The full space is given by a collective index space such that the free part of the action can be written as

$$S_0[\phi] = \frac{1}{2} \sum_{i,j} \phi_i G_{0;i,j}^{-1} \phi_j. \quad (\text{B11})$$

The collective index i summarizes all possible field labels of the considered model. For (B10) $i = (\pm, \tau, x_i, \sigma)$ where $i = (+, \tau, x_i, \sigma)$ labels $\bar{\psi}_{x_i,\sigma}(\tau)$ and $i = (-, \tau, x_i, \sigma)$ labels $\psi_{x_i,\sigma}(\tau)$. The inverse noninteracting two-point correlation function $G_{0;i,j}^{-1}$ is therefore defined in this collective index space with properties discussed in the following.

2. Dyson-Schwinger equations

We start with the most general form of the action of a many-body system with arbitrary two-body interactions:

$$S[\phi] = \frac{1}{2} \phi_{i_1} G_{0;i_1,i_2}^{-1} \phi_{i_2} + \frac{1}{4!} V_{i_1,\dots,i_4} \phi_{i_1} \phi_{i_2} \phi_{i_3} \phi_{i_4},$$

$$Z = \int d(\phi) e^{-S[\phi]}. \quad (\text{B12})$$

The fields ϕ_i are either complex numbers if they represent bosonic degrees of freedom or anticommuting Grassmann

numbers for fermionic degrees of freedom. They are labeled by a single collective index i , which summarizes all possible labels for the fields as introduced in Sec. 1. The action can be formally defined on a lattice or in continuous space, where \mathbf{x} is taken to be a discrete variable or a continuous variable, respectively. The inverse of the noninteracting Greens function G_0^{-1} should be thought of as a symmetric/antisymmetric matrix (for bosons/fermions) in the space of the collective index i and the matrix elements of the two-body interaction are given by a fully symmetric/antisymmetric tensor V . Summation over repeated indices is implicitly assumed.

The Dyson-Schwinger equation for model (B12) can be derived by introducing the generating functional of the n -point correlation functions:

$$Z[J] = \int d(\phi) e^{-S[\phi] + \sum_i J_i \phi_i}. \quad (\text{B13})$$

For bosons the source fields J_i are complex numbers, while for fermions they are Grassmann numbers anticommuting with itself and with the fields ϕ_i . The measure of the functional integral is denoted by $d(\phi)$. All n -point correlation functions can be generated by functional derivatives of the generating functional with respect to the source fields,

$$G_{i_1,\dots,i_n}^{(n)} = \langle \phi_{i_1} \dots \phi_{i_n} \rangle = \frac{1}{Z} \frac{\delta^n Z[J]}{\delta J_{i_1} \dots \delta J_{i_n}} \Big|_{J=0}. \quad (\text{B14})$$

The Dyson-Schwinger equation is derived by considering a linear shift Δ of a single field variable in the functional integral for the generating functional. For fermions, Δ has to be a Grassmann number, while for bosons, Δ is a complex number. The elements in the functional integral for the generating functional transform under this shift as

$$\begin{aligned} \phi_{i_1} &\rightarrow \phi_{i_1} + \Delta, \\ d(\phi) &\rightarrow d(\phi), \\ S[\phi] &\rightarrow S[\phi] + \Delta \frac{\delta S[\phi]}{\delta \phi_{i_1}} + \mathcal{O}(\Delta^2). \end{aligned} \quad (\text{B15})$$

Therefore the generating functional is given by

$$\begin{aligned} Z[J] &= \int d(\phi) e^{-S[\phi] + \sum_i J_i \phi_i - \Delta \frac{\delta S[\phi]}{\delta \phi_{i_1}} \pm \Delta J_{i_1} + \mathcal{O}(\Delta^2)} \\ &= \int d(\phi) \left(1 + \Delta \left[\pm J_{i_1} - \frac{\delta S[\phi]}{\delta \phi_{i_1}} \right] + \mathcal{O}(\Delta^2) \right) \\ &\quad \times e^{-S[\phi] + \sum_i J_i \phi_i}. \end{aligned} \quad (\text{B16})$$

Here and in the following, the upper sign in \pm or \mp is for the bosonic case where the lower sign is for the fermionic case. The differential form of the Dyson-Schwinger equation is obtained by equating the above expression in powers of Δ ,

$$\left(\pm J_{i_1} - \frac{\delta S}{\delta \phi_{i_1}} \left[\frac{\delta}{\delta J} \right] \right) Z[J] = 0. \quad (\text{B17})$$

This is a functional integro-differential equation for the generating functional $Z[J]$. This equation can be formally solved by using the Taylor series expansion of the generating

functional in terms of the source fields J_i around $J_i = 0$,

$$Z[J] = \sum_n \frac{1}{n!} \sum_{i_1, \dots, i_n} G_{i_1, \dots, i_n}^{(n)} J_{i_1} \dots J_{i_n}. \quad (\text{B18})$$

The relations between the expansion coefficients, i.e., the n -point correlation functions, can be obtained by successive differentiation of (B17) with respect to the source fields J_i and setting the sources to $J_i = 0$ afterwards. This yields an infinite tower of integral equations for the n -point correlation functions. The equation obtained by differentiating (B17) once is given by

$$\pm G_{0; i_1, i_3}^{-1} G_{i_3, i_2} + \frac{1}{6} V_{i_1, i_3, i_4, i_5} G_{i_5, i_4, i_3, i_2}^{(4)} = \pm \delta_{i_1, i_2}. \quad (\text{B19})$$

This equation relates the two-point correlation function with the four-point correlation function. The four-point correlation function can be split into a disconnected part and a connected part which on the other hand can be factorized into a contribution coming from the two-point correlation function and a genuine four-point contribution, the four-point vertex function. Therefore we rewrite (B19) such that it relates the two-point correlation function G with the four-point vertex function Γ . In principle, this can be done by introducing further generating functionals for one-particle irreducible correlation functions but as we only need the connection between correlation functions on the four-point level we will directly introduce the relations between them.

The connected four-point correlation function $G_c^{(4)}$ is given by

$$\begin{aligned} G_{c; i_1, i_2, i_3, i_4}^{(4)} &= G_{i_1, i_2, i_3, i_4}^{(4)} - G_{i_1, i_2} G_{i_3, i_4} \\ &\mp G_{i_1, i_3} G_{i_2, i_4} - G_{i_1, i_4} G_{i_2, i_3} \end{aligned} \quad (\text{B20})$$

and the four-point vertex function is related to $G_c^{(4)}$ by

$$\Gamma_{1,2,3,4} = -G_{1,5}^{-1} G_{2,6}^{-1} G_{3,7}^{-1} G_{4,8}^{-1} G_{c; 5,6,7,8}^{(4)}. \quad (\text{B21})$$

Here and in the following, we use the short hand notation $i_n = n$ for the collective index i_n . Plugging this relations into (B19) and solving for the inverse of the two-point correlation function, we obtain

$$\begin{aligned} G_{0; 1,2}^{-1} &= G_{0; 1,2}^{-1} - \Sigma_{1,2}, \\ \Sigma_{1,2} &= \mp \frac{1}{2} V_{1,2,3,4} G_{4,3} + \frac{1}{6} V_{1,3,4,5} G_{5,6} G_{4,7} G_{3,8} \Gamma_{6,7,8,2}. \end{aligned} \quad (\text{B22})$$

The self-energy $\Sigma_{1,2}$ has been introduced as a short hand notation for the contributions coming from the interaction part. The above equation is a single equation for two unknown correlation functions and therefore constitutes an underdetermined set of equations. In the following section, we derive a closed set of equations.

3. Functional closure of Dyson-Schwinger equations

Based on the Dyson-Schwinger equation (B22), which relates the inverse two-point correlation function with the four-point vertex function, we derive a closed set of functional integro-differential equations. The solution of this set of differential equations gives direct access to the two-

point correlation function G and to the four-point vertex function Γ .

We start the derivation with the identity

$$\begin{aligned} \frac{\delta G_{0; 3,4}^{-1}}{\delta G_{0; 3,4}^{-1}} &= \frac{\delta}{\delta G_{0; 3,4}^{-1}} \left[\frac{1}{Z[G_0^{-1}]} \int d(\phi) e^{-S[\phi, G_0^{-1}]} \phi_2 \phi_1 \right] \\ &= \frac{1}{2} G_{3,4} G_{1,2} - \frac{1}{2} G_{1,2,3,4}^{(4)}. \end{aligned} \quad (\text{B23})$$

We have used that

$$\frac{\delta G_{0; 1,2}^{-1}}{\delta G_{0; 3,4}^{-1}} = \frac{1}{2} (\delta_{1,3} \delta_{2,4} \pm \delta_{1,4} \delta_{2,3}). \quad (\text{B24})$$

This functional derivative identity together with the relation between the correlation functions (B20) yields

$$G_{1,2,3,4}^{(4)} = -2 \frac{\delta G_{1,2}}{\delta G_{0; 3,4}^{-1}} + G_{1,2} G_{3,4}. \quad (\text{B25})$$

The four-point vertex function can also be written as a functional derivative with respect to G_0^{-1} by plugging the above identity (B25) into the definition of the four-point vertex function (B21). The final result is

$$\Gamma_{1,2,3,4} = 2 G_{3,5}^{-1} \frac{\delta \Sigma_{1,2}}{\delta G_{0; 5,6}^{-1}} G_{6,4}^{-1}, \quad (\text{B26})$$

where we have used the functional chain rule

$$\frac{\delta G_{1,2}}{\delta G_{0; 3,4}^{-1}} = -G_{1,5} \frac{\delta G_{5,6}^{-1}}{\delta G_{0; 3,4}^{-1}} G_{6,2}. \quad (\text{B27})$$

Up to now, all identities are only based on the general rules of functional differentiation and are not specific to any form of the action $S[\phi]$. To make the connection to the considered model (B12) we can in principle use the identity (B26) in the Dyson-Schwinger equation (B22) to define a coupled set of equations for a functional $G[G_0]$. Numerically more favorable is a universal function $\Gamma[G]$. Therefore, in the following, we will use the self-energy $\Sigma_{1,2}$ obtained from the Dyson-Schwinger equation (B22) and plug this expression into the identity (B26).

We obtain the following expression after a long but straightforward calculation:

$$\begin{aligned} \Gamma_{1,2,3,4} &= V_{1,2,3,4} - \frac{1}{2} V_{1,2,5,6} G_{5,8} G_{6,7} \Gamma_{7,8,3,4} \\ &\mp \frac{1}{2} V_{1,3,5,6} G_{5,8} G_{6,7} \Gamma_{7,8,2,4} \\ &\mp \frac{1}{2} V_{1,4,5,6} G_{5,8} G_{6,7} \Gamma_{7,8,3,2} \\ &+ \frac{1}{2} V_{1,5,6,7} G_{7,10} \Gamma_{10,12,3,4} G_{12,11} G_{5,8} G_{6,9} \Gamma_{8,2,11,9} \\ &+ \frac{1}{3} V_{1,7,8,9} G_{9,10} G_{8,11} G_{7,12} G_{3,5}^{-1} \frac{\delta \Gamma_{10,2,11,12}}{\delta G_{0; 5,6}^{-1}} G_{6,4}^{-1}. \end{aligned} \quad (\text{B28})$$

The last term can be simplified by noting that second order functional derivatives commute. The following commutator

identity can be derived using this property,

$$\begin{aligned}
& \left[G_{11,5}^{-1} G_{6,12}^{-1} \frac{\delta \Gamma_{10,2,3,4}}{\delta G_{0,5,6}^{-1}} - G_{3,5}^{-1} G_{6,4}^{-1} \frac{\delta \Gamma_{10,2,11,12}}{\delta G_{0,5,6}^{-1}} \right] \\
&= 2G_{11,5}^{-1} G_{6,12}^{-1} \frac{\delta}{\delta G_{0,5,6}^{-1}} \left[G_{3,9}^{-1} \frac{\delta \Sigma_{10,2}}{\delta G_{0,9,13}^{-1}} G_{13,4}^{-1} \right] \\
&\quad - 2G_{3,5}^{-1} G_{6,4}^{-1} \frac{\delta}{\delta G_{0,5,6}^{-1}} \left[G_{11,9}^{-1} \frac{\delta \Sigma_{10,2}}{\delta G_{0,9,13}^{-1}} G_{13,12}^{-1} \right] \\
&= -\frac{1}{2} \Gamma_{3,\alpha,11,12} G_{\alpha,\beta} \Gamma_{10,2,\beta,4} - \frac{1}{2} \Gamma_{11,4,\alpha,12} G_{\alpha,\beta} \Gamma_{10,2,3,\beta} \\
&\quad + \frac{1}{2} \Gamma_{11,\alpha,3,4} G_{\alpha,\beta} \Gamma_{10,2,\beta,12} + \frac{1}{2} \Gamma_{12,\alpha,3,4} G_{\alpha,\beta} \Gamma_{10,2,11,\beta}.
\end{aligned} \tag{B29}$$

This identity is used to rewrite the last term in (B28) such that the four-point vertex is given by

$$\begin{aligned}
\Gamma_{1,2,3,4} &= V_{1,2,3,4} - \frac{1}{2} V_{1,2,5,6} G_{5,8} G_{6,7} \Gamma_{7,8,3,4} \\
&\quad \mp \frac{1}{2} V_{1,3,5,6} G_{5,8} G_{6,7} \Gamma_{7,8,2,4} \\
&\quad \mp \frac{1}{2} V_{1,4,5,6} G_{5,8} G_{6,7} \Gamma_{7,8,3,2} \\
&\quad + \frac{1}{3} V_{1,5,6,7} G_{5,8} \frac{\delta \Gamma_{8,2,3,4}}{\delta G_{0,6,7}^{-1}} \\
&\quad + \frac{1}{6} V_{1,5,6,7} G_{7,10} \Gamma_{10,12,3,4} G_{12,11} G_{5,8} G_{6,9} \Gamma_{8,2,11,9} \\
&\quad \pm \frac{1}{6} V_{1,5,6,7} G_{7,10} \Gamma_{10,12,2,4} G_{12,11} G_{5,8} G_{6,9} \Gamma_{8,3,11,9} \\
&\quad \pm \frac{1}{6} V_{1,5,6,7} G_{7,10} \Gamma_{10,12,3,2} G_{12,11} G_{5,8} G_{6,9} \Gamma_{8,4,11,9}.
\end{aligned} \tag{B30}$$

Formally, (B22) and (B30) form a closed set of equations where the four-point vertex function should be thought of as a functional of the inverse of the noninteracting two-point correlation function. It is much more desirable to define the four-point vertex function as a functional of the two-point correlation function. This functional is obtained by using again the functional chain rule,

$$\frac{\delta}{\delta G_{0,6,7}^{-1}} = \left(\frac{\delta G_{9,10}}{\delta G_{0,6,7}^{-1}} \right) \frac{\delta}{\delta G_{9,10}}. \tag{B31}$$

With (B25) the first term in the product can be expanded to

$$\begin{aligned}
\frac{\delta G_{9,10}}{\delta G_{0,6,7}^{-1}} &= \frac{1}{2} G_{9,a} G_{10,b} G_{6,c} G_{7,d} \Gamma_{a,b,c,d} \\
&\quad - \frac{1}{2} G_{7,9} G_{6,10} \mp \frac{1}{2} G_{7,10} G_{6,9}.
\end{aligned} \tag{B32}$$

This relations transforms (B30) into a definition of the four-point vertex function as a universal functional $\Gamma[G]$ in the language of a functional integro-differential equation. The complete set of closed Dyson-Schwinger equations is given by

$$\begin{aligned}
G_{1,2}^{-1} &= G_{0,1,2}^{-1} - \Sigma_{1,2}, \\
\Sigma_{1,2} &= \mp \frac{1}{2} V_{1,2,3,4} G_{4,3} + \frac{1}{6} V_{1,3,4,5} G_{5,6} G_{4,7} G_{3,8} \Gamma_{6,7,8,2}, \\
\Gamma_{1,2,3,4} &= V_{1,2,3,4} - \frac{1}{2} V_{1,2,5,6} G_{5,8} G_{6,7} \Gamma_{7,8,3,4} \\
&\quad \mp \frac{1}{2} V_{1,3,5,6} G_{5,8} G_{6,7} \Gamma_{7,8,2,4} \\
&\quad \mp \frac{1}{2} V_{1,4,5,6} G_{5,8} G_{6,7} \Gamma_{7,8,3,2} \\
&\quad + \frac{1}{6} V_{1,5,6,7} G_{7,10} \Gamma_{10,12,3,4} G_{12,11} G_{5,8} G_{6,9} \Gamma_{8,2,11,9} \\
&\quad \pm \frac{1}{6} V_{1,5,6,7} G_{7,10} \Gamma_{10,12,2,4} G_{12,11} G_{5,8} G_{6,9} \Gamma_{8,3,11,9} \\
&\quad \pm \frac{1}{6} V_{1,5,6,7} G_{7,10} \Gamma_{10,12,3,2} G_{12,11} G_{5,8} G_{6,9} \Gamma_{8,4,11,9} \\
&\quad \mp \frac{1}{3} V_{1,5,6,7} G_{5,8} G_{6,9} G_{7,10} \frac{\delta \Gamma_{8,2,3,4}}{\delta G_{9,10}} \\
&\quad + \frac{1}{6} V_{1,5,6,7} G_{5,8} G_{6,11} G_{7,14} \Gamma_{11,12,13,14} \\
&\quad \times G_{12,9} G_{13,10} \frac{\delta \Gamma_{8,2,3,4}}{\delta G_{9,10}}.
\end{aligned} \tag{B33}$$

The equations are diagrammatically depicted in Fig. 2.

APPENDIX C: NUMERICAL IMPLEMENTATION

In this section, we discuss the numerical implementation for the solution of the functional integro-differential equation in (B33) for the \mathcal{Z}_2 symmetric ϕ^4 model in 2D, cf. (B4). Thus, in the following, we consider model (B12) for the case where the collective index i just consists of the labels of the discrete lattice sites $i = (\mathbf{x}_i)$ of the 2D square lattice. We will see in the following that adding additional field labels to the collective index i in principle does not change the algorithm but complicates the already complex bookkeeping of indices in the algorithm.

For model (12) $G_{0;i,j}^{-1} = -\square_{i,j} + m^2 \delta_{i,j}$, where \square is the discretized Laplace operator in D dimensions and the fully symmetric tensor is given by the on-site interaction $V_{i,j,k,l} = \lambda \delta_{i,j} \delta_{i,k} \delta_{i,l}$. We consider the construction of the universal functional $\Gamma[G]$ through the solution of the vertex equation in (B33) in momentum space. In the following, the momentum variables are denoted by $\mathbf{p}_i = i$ and the linear combination of momentum variables by, e.g., $\mathbf{p}_i + \mathbf{p}_j = i + j$. In this representation, the integro-differential equation in (B33) can

be written as

$$\begin{aligned} \Gamma_{1,2,3,4} &= \lambda \delta_{1+2+3,-4} - \frac{\lambda}{2} \sum_{5,6,7} G_{5,6} [G_{1+2-5,7} \Gamma_{-7,-6,3,4} + G_{1+3-5,7} \Gamma_{-7,-6,2,4} + G_{1+4-5,7} \Gamma_{-7,-6,3,2}] \\ &+ \frac{\lambda}{6} \sum_{5,\dots,12} G_{1-5-7,11} G_{5,6} G_{7,8} G_{9,10} [\Gamma_{-6,2,-9,-8} \Gamma_{-11,-10,3,4} + \Gamma_{-6,3,-9,-8} \Gamma_{-11,-10,2,4} + \Gamma_{-6,4,-9,-8} \Gamma_{-11,-10,3,2}] \\ &- \frac{\lambda}{3} \sum_{5,\dots,9} G_{1-5-6,7} G_{5,8} G_{6,9} \frac{\delta \Gamma_{-7,2,3,4}}{\delta G_{8,9}} + \frac{\lambda}{6} \sum_{5,\dots,13} G_{1-5-6,7} G_{5,8} G_{6,9} \Gamma_{-8,-11,-13,-9} G_{10,11} G_{12,13} \frac{\delta \Gamma_{-7,2,3,4}}{\delta G_{10,12}}. \end{aligned} \quad (\text{C1})$$

The universal functional $\Gamma[G]$ has to be constructed as the solution of (C1) for arbitrary $G \in \mathbb{R}^{L \times L}$, i.e., not restricted to the subspace of physical correlation functions which satisfy translational symmetry. Thus, going into the momentum representation does not diagonalize the two-point correlation function, $G(1, 2) \neq G(1) \delta_{1,-2}$ and also $\Gamma(1, 2, 3, 4) \neq \Gamma(1, 2, 3, -1 - 2 - 3) \delta_{4,-1-2-3}$. Only the evaluation of $\Gamma[G]$ in the physical subspace of translational invariant solutions will give a translational invariant four-point vertex function $\Gamma(1, 2, 3, 4) = \Gamma(1, 2, 3, -1 - 2 - 3) \delta_{4,-1-2-3}$.

We show in the following that it is possible to construct the solution in the absence of translational symmetry and simultaneously evaluate the solution $\Gamma[G]$ only in the restricted physical subspace of translational invariant G .

1. Homotopy analysis method

In this section, the semianalytic HAM is used to solve the functional integro-differential equation (C1). As discussed in Sec. III the starting point of the HAM is the construction of the homotopy

$$(1 - q) \mathcal{L}[\phi[G, q] - u_{\Gamma,0}[G]] + q c_0 \mathcal{N}[\phi[G, q]] = 0. \quad (\text{C2})$$

$\mathcal{N}[\Gamma[G]] = 0$ is the nonlinear differential operator defining (C1) and \mathcal{L} is an arbitrary linear operator with the

property $\mathcal{L}[0] = 0$. The homotopy (C2) includes the deformation parameter $q \in [0, 1]$, which deforms the solution of \mathcal{L} , $\phi[G, 0] = u_{\Gamma,0}[G]$, at $q = 0$ to the solution of the differential equation (C1), $\phi[G, 1] = \Gamma[G]$, at $q = 1$. $u_{\Gamma,0}[G]$ is the initial guess for the solution of $\mathcal{N}[\Gamma[G]] = 0$. The convergence control parameter c_0 controls the rate at which the deformation takes place. The HAM tries to find the solution of (C2) through a Taylor series expansion in q , i.e., $\phi[G, q] = u_{\Gamma,0}[G] + \sum_{m=1} u_{\Gamma,m}[G] q^m$. The expansion coefficients are given by $u_{\Gamma,m}[G] = \phi^{(m)}[G, q = 0]/m!$ and can be obtained by the m th derivative of (C2) with respect to q . Therefore the HAM gives a series solution of the functional integro-differential equation (C1) in terms of the deformation coefficients $u_{\Gamma,m}[G]$,

$$\Gamma[G] = u_{\Gamma,0}[G] + \sum_{m=1} u_{\Gamma,m}[G]. \quad (\text{C3})$$

In the following, we use the easiest possible linear operator $\mathcal{L}[\phi[G, q] - u_{\Gamma,0}[G]] = \phi[G, q] - u_{\Gamma,0}[G]$, which we ultimately use in the final calculations. More complicated linear operators, such as the ladder summation, will be left to future work. Differentiating (C1) m times with respect to q and setting $q = 0$ gives the m th-order deformation equation

$$\begin{aligned} u_{\Gamma,m}(\mathbf{p}) &= \chi_m u_{\Gamma,m-1}(\mathbf{p}) - c_0 \left[u_{\Gamma,m-1}(\mathbf{p}) - \lambda \delta(\mathbf{p}) \tilde{\chi}_m + \frac{\lambda}{2} \sum_c \sum_{5,6,7} K_c^{(1)}(\mathbf{p}_c, 5, 6, 7) u_{\Gamma,m-1}(-7, -6, \mathbf{p}_{\bar{c}}) \right. \\ &- \frac{\lambda}{6} \sum_c \sum_{5,\dots,11} K_c^{(2)}(\mathbf{p}_c, 5, \dots, 11) \sum_{k=0}^{m-1} u_{\Gamma,k}(-11, -10, \mathbf{p}_{\bar{c}}) u_{\Gamma,m-1-k}(-6, p_c, -9, -8) \\ &+ \frac{\lambda}{3} \sum_{5,\dots,9} K^{(3)}(1, 5, \dots, 9) \frac{\delta u_{\Gamma,m-1}(-7, 2, 3, 4)}{\delta G_{8,9}} \\ &\left. - \frac{\lambda}{6} \sum_{5,\dots,13} K^{(4)}(1, 5, \dots, 13) \sum_k^{m-1} u_{\Gamma,m-1-k}(-8, -11, -13, -9) \frac{\delta u_{\Gamma,k}(-7, 2, 3, 4)}{\delta G_{10,12}} \right]. \end{aligned} \quad (\text{C4})$$

We have introduced the following notations: (1) $u_{\Gamma,m}(\mathbf{p})$ denotes the deformation $u_{\Gamma,m}[G]$ at external variables $\mathbf{p} = (1, 2, 3, 4)$. (2) The sum \sum_c runs over the three possible permutations of external legs, cf. Eq. (C1). We introduce the following abbreviations for the permutations: $s = \{1,2,3,4\}$, $t = \{1,3,2,4\}$, $u = \{1,4,3,2\}$. (3) The contributions coming from G in (C1) are collected in the kernel

functions $K_c^{(i)}$, $i \in \{1, 2\}$ and $K^{(3)}$, $K^{(4)}$. The various kernel functions are explicitly summarized in Appendix D. (4) The projection of the 4D vector of external variables \mathbf{p} onto a 2D subspace and its complement is denoted by \mathbf{p}_c , $\mathbf{p}_{\bar{c}}$, respectively: $\mathbf{p}_{c=s} = (1, 2)$, $\mathbf{p}_{\bar{c}=s} = (3, 4)$; $\mathbf{p}_{c=t} = (1, 3)$, $\mathbf{p}_{\bar{c}=t} = (2, 4)$; $\mathbf{p}_{c=u} = (1, 4)$, $\mathbf{p}_{\bar{c}=u} = (3, 2)$. (5) The projection of the 4D vector of external variables \mathbf{p} onto a

D dimensional vector is denoted by p_c : $p_{c=s} = 2$; $p_{c=t} = 3$; $p_{c=u} = 4$. (6) $\chi_m = 1 - \delta_{m,1}$ and $\tilde{\chi}_m = \delta_{m,1}$. (7) $\delta(\mathbf{p}) = \delta_{4,-1-2-3}$ denotes the momentum conservation at the bare vertex.

The equation for the m -th-order deformation equation is the starting point for the tree expansion developed in Ref. [17] for a truncated functional $\Gamma[G]$. In the next section, we will summarize the main ideas of the tree expansion and extend these ideas to account for the functional derivatives in (C4).

2. Tree expansion

The m th-order deformation equation (C4) gives the m th term in the series solution (C3) of the HAM. In order to calculate the m th deformation, all previous deformations and their functional derivatives have to be known. Neglecting the functional dependence on the unknown G for a moment, already the full storage of a single deformation is a formidable task as the deformations themselves depend on four external indices, which are D -dimensional vectors, i.e., $u_{\Gamma,m}(\mathbf{p})$ is a rank-4D tensor. Including the functional derivatives seems to make a numerical calculation of (C4) an impossible task. The tree expansion developed in Ref. [17] solves this apparently impossible task by a stochastic interpretation. The basic idea of the tree expansion is that in order to calculate the m th-order deformation with (C4), (C4) is used again on the right-hand side to get rid off the explicit dependence of all deformations and functional derivatives with $k < m$. This procedure is recursively repeated until all deformations $u_{\Gamma,m}$ with $m > 0$ are eliminated on the right-hand side. The result is a complicated expression, the tree expansion, which only depends explicitly on the deformation $u_{\Gamma,0}$. We will develop a diagrammatic language which captures all possible terms in the tree expansion and introduce a Monte Carlo algorithm to stochastically sum all terms. Each term in the tree expansion will be represented in the diagrammatic language of rooted trees which will be introduced in the following. Therefore the tree expansion for $u_{\Gamma,m}$ is given by the sum of all possible rooted tree diagrams, which can be constructed with respect to a certain fixed set of rules.

We start the discussion with the rooted tree diagram in Fig. 11(a). It corresponds to a single term in the tree expansion. For the moment, we are neglecting the labeling of the rooted tree and consider only the overall structure of the tree and its corresponding analytic expression. After the general structure is introduced, we discuss its labeling, i.e., how momentum variables and additional labels, e.g., external leg permutations, are taken into account. The rooted tree and the structure of the corresponding analytic expression is obtained from the following procedure.

The uppermost circle, the root of the rooted tree, corresponds to the left-hand side of (C4). In the case of Fig. 11(a), $u_{\Gamma,3}$ should be expanded. The branch, indicated by a straight line, growing from the root leading to two leaves, represented by the circles, diagrammatically depicts that $u_{\Gamma,3}$ is expanded in the first stage with respect to the third line in (C4), i.e.,

$$K_c^{(2)} \sum_{k=0}^{m-1} u_{\Gamma,k} u_{\Gamma,m-1-k}. \quad (\text{C5})$$

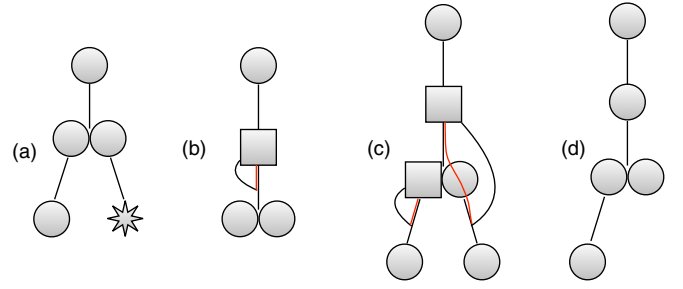


FIG. 11. Examples of rooted tree diagrams, which are constructed by expanding the HAM in the tree expansion. The different diagrammatic elements are explained in the main text and listed in Fig. 12. The rooted trees in (a) and (d) do not include functional derivatives. The rooted trees in (b) and (c) include functional derivatives, which are indicated by the arc lines closing on a branch. The additional red line is introduced for the bookkeeping of excess momenta carried by the functional derivative. The different stages in the tree expansion leading to the rooted trees in (a)–(d) are explained in the main text.

Thus, the branch corresponds to the integral kernel $K_c^{(2)}$ and the two leaves corresponds to the product of deformations $u_{\Gamma,k} u_{\Gamma,m-1-k}$. A single term in the sum over deformations is chosen. In Fig. 11(a), $k = 1$ has been picked leading to $u_{\Gamma,1} u_{\Gamma,1}$. In the second stage, the above procedure is repeated by considering each leaf as a new individual root. In case of Fig. 11(a), the left leaf has been expanded with respect to the second line in (C4), i.e.,

$$K_c^{(1)} u_{\Gamma,0}, \quad (\text{C6})$$

and the right leaf corresponds to the first line, i.e.,

$$\chi_1 u_{\Gamma,0} - c_0 [u_{\Gamma,0} - \lambda \tilde{\chi}_1] = -c_0 [u_{\Gamma,0} - \lambda]. \quad (\text{C7})$$

For that case, there is no contribution from an integral kernel. This is indicated by drawing the leaf as a star instead of a circle. Gathering all contributions, the structure of the analytic expression corresponding to the rooted tree in the example of Fig. 11(a) is

$$K_c^{(2)} K_c^{(1)} u_{\Gamma,0} (-c_0 [u_{\Gamma,0} - \lambda]). \quad (\text{C8})$$

This is a single term in the tree expansion and illustrates that the rooted trees depend explicitly only on the kernel functions and on the initial guess $u_{\Gamma,0}$, which is the starting point of the series solution (C3). The discussion also shows that in (C4) there are five different possibilities to expand $u_{\Gamma,m}$, which lead to the five different branch types. All branch types with their respective leaves are shown in Fig. 12. In the diagrammatic expressions the branch type is determined by the leaves on the lower end of the branch. The branch type in Figs. 12(d) and 12(e) correspond to the expansion with respect to the functional derivative terms. The leaves with functional derivatives are drawn by boxes and the additional dangling line is introduced. It indicates the action of the functional derivative on a consecutive element in the rooted tree.

On the basis of Fig. 11(c), we discuss the structure of the analytic expression corresponding to a rooted tree with functional derivatives. In the first stage of the tree expansion, the root $u_{\Gamma,4}$ is expanded with respect to the branch type

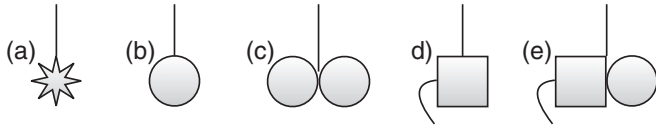


FIG. 12. The possible branch types of the rooted trees. Each branch type corresponds to a single line on the right-hand side of (C4). The straight line, the branch itself, represents the corresponding kernel function $K_c^{(i)}$, $i \in \{1, 2\}$ or $K^{(i)}$, $i \in \{3, 4\}$ for the respective branch type. The star, circle, and box indicate the leaf grown from the branch. They represent the contribution from the deformation $u_{\Gamma,m}$ for the specific branch type. The star contributes no integration variable to the tree, cf. first line in (C4). The box corresponds to a leaf at which a functional derivative is introduced. The branch type can be read off from the combination of leaves grown on the lower end of the branch. The leaf types (c) and (e) consists of two individual single leaves because each can be individually expanded further in the tree expansion. The dangling lines on the leafs of (d) and (e) are representing the not yet completed action of the functional derivative on a consecutive branch.

Fig. 12(d), which includes a single leaf with a functional derivative. The structure of the analytic expression in this expansion stage is given by

$$K^{(3)} \frac{\delta u_{\Gamma,3}}{\delta G}. \quad (\text{C9})$$

In the next stage, $u_{\Gamma,3}$ is expanded with respect to the branch type Fig. 12(e). This gives the analytic expression

$$K^{(3)} \frac{\delta}{\delta G} \left(K^{(4)} \frac{\delta u_{\Gamma,1}}{\delta G} u_{\Gamma,1} \right). \quad (\text{C10})$$

Due to the product rule of functional derivatives there are three possibilities for the action of the outer functional derivative. The first possibility is that the functional derivative is acting on the kernel function of the second expansion stage, i.e., the branch directly after the deformation $u_{\Gamma,3}$ is differentiated. The second possibility is that the outer derivative is acting on the leaf with the functional derivative and therefore a second-order functional derivative is produced. The third possibility is that it acts on the deformation $u_{\Gamma,1}$. From Fig. 11(c), we see that the dangling line is completed to an arc line, which indicates that the derivative introduced in the first stage of the tree expansion is differentiating a branch grown after the leaf without a functional derivative. Therefore the third possibility is represented by the rooted tree in Fig. 11(c) and the analytic expression for the rooted tree in this expansion stage is

$$K^{(3)} K^{(4)} \frac{\delta u_{\Gamma,1}}{\delta G} \frac{\delta u_{\Gamma,1}}{\delta G}. \quad (\text{C11})$$

In the next two expansion stages, the deformations $u_{\Gamma,1}$ are further expanded. In both cases with respect to the branch type Fig. 12(b). This gives the analytic expression

$$K^{(3)} K^{(4)} \frac{\delta}{\delta G} (K_c^{(1)} u_{\Gamma,0}) \frac{\delta}{\delta G} (K_c^{(1)} u_{\Gamma,0}). \quad (\text{C12})$$

Here and in the following, we consider only initial guesses $u_{\Gamma,0}$, which have no explicit G dependence, i.e.,

$$\frac{\delta u_{\Gamma,0}}{\delta G} = 0. \quad (\text{C13})$$

Taking this into account the structure of the analytic expression corresponding to the fully grown root tree in Fig. 11(c) is given by

$$K^{(3)} K^{(4)} \frac{\delta K_c^{(1)}}{\delta G} u_{\Gamma,0} \frac{\delta K_c^{(1)}}{\delta G} u_{\Gamma,0}. \quad (\text{C14})$$

From this discussion, we see that functional derivatives can only act on the branches of a fully grown rooted tree. Nevertheless, in intermediate stages of the tree expansion the functional derivatives can act on the deformations with $u_{\Gamma,m}$, $m > 0$. These have to be expanded further in later stages of the tree expansion and therefore the analytic expression corresponding to a fully grown rooted tree involves only $u_{\Gamma,0}$, kernel functions and functional derivatives of the kernel functions. Moreover, as we see from the above discussion the derivatives can only act on branches, which are grown from a leaf consecutive to a functional derivative leaf. Examples of valid rooted trees with functional derivatives are shown in Figs. 11(b) and 11(c). In these fully grown rooted trees, the dangling lines, which indicate the action of the functional derivative form closed arc lines connecting a functional derivative leaf to a branch. This denotes which branch is differentiated by the functional derivative. We will see later that each branch can only be differentiated a finite amount of times and therefore all possible functional derivatives on all possible branches can be tabulated, cf. Appendix E.

We have introduced the general structure of the rooted trees in the framework of the tree expansion on the basis of the examples in Fig. 11. In the following, we discuss the labeling and the specific analytic expressions of the diagrammatic elements in the rooted tree diagrams. The universal functional $\Gamma[G]$ is a functional with respect to an arbitrary $G \in \mathbb{R}^{L \times L}$, which is not necessarily defined inside the physical, translational invariant subspace. Nevertheless, we finally want to evaluate $\Gamma[G]$ in the subspace of physical G . We showed that $\Gamma[G]$ can be constructed by drawing all possible rooted tree diagrams in the tree expansion of the HAM. Therefore, in order to evaluate $\Gamma[G]$ at a physical G , the diagrammatic elements of the rooted tree diagrams, i.e., the kernel functions and their derivatives have to be build up from the physical, translational invariant two-point correlation functions. In the following, we show how this leads to the correct labeling of the rooted tree diagrams.

Consider the rooted tree diagram in the tree expansion for $u_{\Gamma,3}$ depicted in Fig. 11(d). We fix the external momentum of the root, $u_{\Gamma,3}(\mathbf{p})$, to be $\mathbf{p} = (p_1, p_2, p_3, -p_1 - p_2 - p_3)$, i.e., the rooted tree diagram is evaluated inside the translational invariant subspace. The first stage in the tree expansion for the rooted tree in Fig. 11(d) is graphically illustrated in Fig. 13(a). In the example, the expansion is performed in the t-permutation channel, cf. (C4). The analytic expression corresponding to this expansion stage is diagrammatically illustrated on the right-hand side of the arrow in Fig. 13(a) and can be read off as

$$\begin{aligned} & \sum_{5,6,7} K_{c=t}^{(1)}(\mathbf{p}_{c=t}, 5, 6, 7) u_{\Gamma,2}(-7, -6, \mathbf{p}_{\bar{c}=\bar{t}}) \\ & = G_{5,6} G_{1+3-5,7} u_{\Gamma,2}(-7, -6, 2, 4) \\ & \stackrel{G=G_{\text{phys}}}{=} G_5 G_{1+3-5} u_{\Gamma,2}(\mathbf{p}'). \end{aligned} \quad (\text{C15})$$

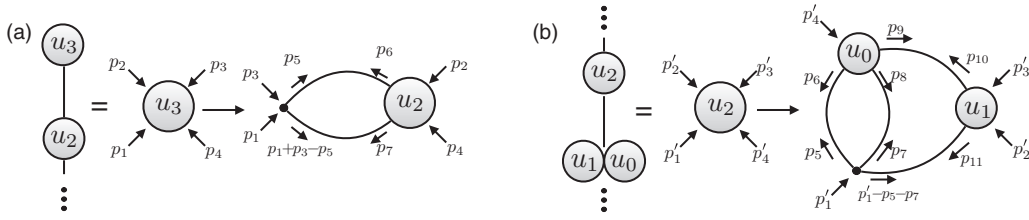


FIG. 13. Two consecutive stages of expansions in the tree expansion leading to the full rooted tree in Fig. 11(d). The two-point correlation functions contribution to the kernel are not yet evaluated in the physical, translational invariant subspace. Therefore G still depends on two momentum variables, which are indicated by two arrows on top of the G lines. The new external momentum carried by the leafs is determined by the kernel functions in (C4) and the specific random permutation of external legs picked for this expansion stage. Diagrammatically, the contributing kernel functions together with the respective deformations are depicted on the right-hand side of the arrow. (a) The deformation $u_{\Gamma,3}$ is expanded with respect to the second line in (C4) leading to a new leaf, $u_{\Gamma,2}$. The branch corresponds to the kernel function depending on two two-point correlation functions, which lead to an evaluation of the lower-order deformation at a new external momentum. In this example, the t channel is considered. (b) In the next expansion stage, the leaf $u_{\Gamma,2}$ is expanded further with respect to the third line in (C4) in the u permutation. In this case, the kernel function depends on four two-point correlation functions and the leafs corresponds to two lower order deformations each evaluated at a new external momentum.

Here and in the following, summation over repeated indices is assumed implicitly. Obviously, the kernel function can be evaluated in the physical subspace of translational invariant G , $G_{\text{phys},1,2} = G_1 \delta_{1,-2}$. Consequently, the new external momentum for $u_{\Gamma,2}(\mathbf{p}')$ is $\mathbf{p}' = (p'_1, p'_2, p'_3, p'_4) = (p_1 + p_3 - p_5, p_5, p_2, -p_1 - p_2 - p_3)$ and therefore momentum conservation is fulfilled and the procedure of the tree expansion can be recursively repeated without leaving the physical subspace.

The same holds for the expansion with respect to the branch type Fig. 12(c). For the example of Fig. 11(d), the second stage of the tree expansion is illustrated in Fig. 13(b). In this case, assuming that the u permutation has been chosen,

$$\begin{aligned} & \sum_{5, \dots, 11} K_u^{(2)}(\mathbf{p}'_{c=u}, 5, \dots, 11) u_{\Gamma,1}(-11, -10, \mathbf{p}'_{\bar{c}=\bar{u}}) \\ & \quad \times u_{\Gamma,0}(-6, p_{c=u}, -9, -8) \\ & = G_{1'-5-7,11} G_{5,6} G_{7,8} G_{9,10} u_{\Gamma,1}(-11, -10, 3', 2') \\ & \quad \times u_{\Gamma,0}(-6, 4', -9, -8) \\ & \stackrel{G=G_{\text{phys}}}{=} G_5 G_6 G_{-4'-5+6} G_{1'+4'-6} u_{\Gamma,0}(\mathbf{p}'') u_{\Gamma,1}(\mathbf{p}'''). \quad (\text{C16}) \end{aligned}$$

The external momentum variables for the leafs $u_{\Gamma,0}(\mathbf{p}'')$ and $u_{\Gamma,1}(\mathbf{p}''')$ are after the evaluation of G in the physical subspace, $\mathbf{p}'' = (p_5, p'_4, -p_6, -p'_4 - p_5 + p_6)$ and $\mathbf{p}''' = (p'_1 + p'_4 - p_6, p_6, p'_3, p'_2)$. Therefore the evaluation of the deformations $u_{\Gamma,0}$, $u_{\Gamma,1}$ is again in the physical subspace. We are choosing the convention that the leaf on the left-hand side of the grown branch of type Fig. 12(c) corresponds to the deformation depending on two external variables. In the example, the deformation $u_{\Gamma,1}$, depending on two external variables, is represented by the left leaf, whereas $u_{\Gamma,0}$, depending on one external variables, is represented by the right leaf, cf. Fig. 13(b).

In conclusion, we see from this example that there are no further complications in evaluating the rooted tree diagram at $G = G_{\text{phys}}$ if the diagram contains no elements with functional derivatives. In this case, the only information needed in each expansion stage is (1) the external momentum variables of the leaf which is expanded, (2) the branch type into which the leaf is expanded, and (3) the internal momentum variables

over which is integrated. This provides enough information to compute in each expansion stage the new external momentum variables for the newly grown leafs and therefore the tree expansion can be carried out recursively.

Rooted tree diagrams with elements of type Figs. 12(d) and 12(e) need some further consideration. As an example consider Fig. 11(b), which contains a functional derivative.

As in the previous example, the rooted tree is evaluated in the physical subspace by fixing the external momentum of the root to be $\mathbf{p} = (p_1, p_2, p_3, -p_1 - p_2 - p_3)$ and evaluate the kernel function corresponding to the branch of the corresponding branch type, Fig. 12(d), at translational invariant G . This is illustrated in Fig. 14(a).

$$\begin{aligned} & \sum_{5, \dots, 9} K^{(3)}(1, 5, \dots, 9) \frac{\delta u_{\Gamma,1}(-7, 2, 3, 4)}{\delta G_{8,9}} \\ & = G_{1-5-6,7} G_{5,8} G_{6,9} \frac{\delta u_{\Gamma,1}(-7, 2, 3, -1-2-3)}{\delta G_{8,9}} \\ & \stackrel{G=G_{\text{phys}}}{=} G_{1-5-6} G_5 G_6 \frac{\delta u_{\Gamma,1}(\mathbf{p}')}{\delta G_{-5,-6}}. \quad (\text{C17}) \end{aligned}$$

The additional arrowheads on the two-point correlation function lines in Fig. 14(a) are indicating the connection to the functional derivative. Note that only the G lines contributing to the kernel function are evaluated in the physical subspace. The functional derivative still depends on two momentum variables. We will show later how this has to be understood by considering the differentiation of a kernel function. The G lines without additional arrowheads are connected to the deformation such that the momentum carried by this line is contributing to the new external momentum of the newly grown leaf. In contrast to the previous examples without functional derivatives, the external momentum $\mathbf{p}' = (p'_1, p'_2, p'_3, p'_4) = (1-5-6, 2, 3, -1-2-3)$ for $u_{\Gamma,1}$ does not automatically satisfy momentum conservation after the kernel function has been evaluated in the physical subspace of translational invariant G . There is an excess momentum carried by the functional derivative. Only if this excess momentum is taken correctly into account the momentum variables sum up to zero. The

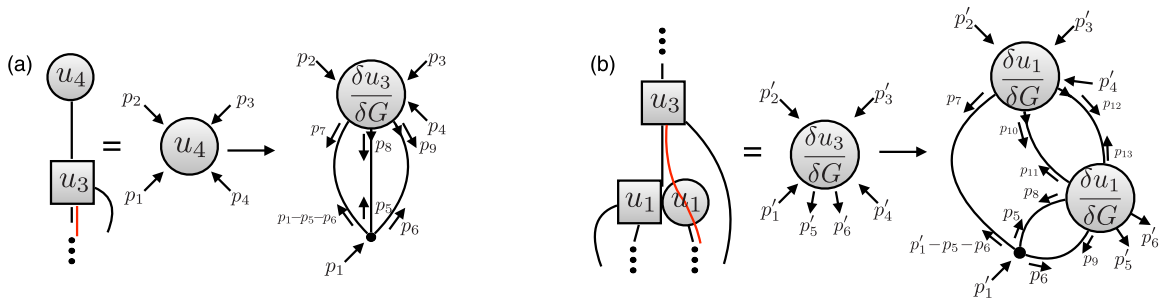


FIG. 14. Two consecutive stages in the tree expansion leading to the full rooted tree in Fig. 11(c). In this case both expansion stages involve functional derivatives. In order to indicate the correct momentum conservation (C19), the legs of the leaf corresponding to the momentum variables of the functional derivatives carry additional arrows. (a) The first stage of the expansion of $u_{\Gamma,4}$ is carried out with respect to the fourth line in (C4). The dangling line on the leaf indicates the functional derivative whereas the red line indicates the bookkeeping of excess momentum carried by the derivative as discussed in the main text. (b) In the second stage of the tree expansion, $u_{\Gamma,3}$ is expanded with respect to the fifth line. The dangling functional derivative is not directly acting on the newly grown branch. Therefore the red bookkeeping line goes straight through the leaf. In the diagrammatic expansion for the kernel, this is indicated as an additional derivative for the leaf on the lower right-hand side, cf. the fifth line in (C4), which includes only the derivative of the upper leaf.

correct momentum conservation at the functional derivative terms can be found from the following argument.

The functional derivative of the four-point vertex function with respect to G gives a term which account for correlation functions on the six-point level. We write this as

$$\begin{aligned} \mathcal{O}_{\Gamma^{(6)}}(i_1, i_2, i_3, i_4; i_5, i_6) & \\ & \equiv \frac{\delta \Gamma(i_1, i_2, i_3, i_4)}{\delta G(i_5, i_6)} \\ & = \frac{\delta \Gamma(p_1, p_2, p_3, p_4)}{\delta G(p_5, p_6)} e^{-i \sum_{n=1}^4 p_n i_n} e^{i \sum_{n=5}^6 p_n i_n}. \quad (\text{C18}) \end{aligned}$$

In the subspace of physical correlation functions, $\mathcal{O}_{\Gamma^{(6)}}$ depends only on the relative distances between the lattice sites i_1, \dots, i_6 . Therefore, in order to evaluate rooted trees with functional derivatives in the translational invariant subspace, the correct momentum conservation at the functional derivative is $\delta(p_1 + p_2 + p_3 + p_4 - p_5 - p_6)$. We will also need the more general result for the momentum conservation with multiple functional derivatives

$$\begin{aligned} \mathcal{O}_{\Gamma^{(4+N)}}(p_1, p_2, p_3, p_4; l_0, l_1, \dots, l_{2N}, l_{2N-1}) & \\ & = \frac{\delta \Gamma(p_1, p_2, p_3, p_4)}{\delta G(l_0, l_1) \dots G(l_{2N}, l_{2N-1})} \\ & \times \delta \left(p_1 + p_2 + p_3 + p_4 - \sum_{n=0}^{2N-1} l_n \right). \quad (\text{C19}) \end{aligned}$$

The functional derivative terms explicitly break momentum conservation on the four-point level but on a higher correlation function level it must always be satisfied with respect to the extended momentum conservation rule (C19). The additional arrowheads on the G lines, cf. Fig. 14(a), can also be viewed as indicating that these momenta are contributing with a minus sign in the extended momentum conservation rule. This consideration shows that (C17) is a valid projection into the physical subspace and the tree expansion can now be carried on if the momentum conservation rule (C19) is taken into account.

Diagrammatically the excess momenta carried by the functional derivatives are depicted as the previously introduced additional arcs which originate from leafs with functional derivatives and close on a branch, cf. Fig. 11(c). We show in the following that once an arc closes on a branch, i.e., after the functional derivative acted on a kernel function, momentum conservation will be automatically restored on the four-point level.

We consider the example in Fig. 11(c). The analytic expression obtained in the first stage of the expansion of $u_{\Gamma,4}$ at fixed external momentum variables compatible with translational invariance $\mathbf{p} = (p_1, p_2, p_3, -p_1 - p_2 - p_3)$ is already given in (C17) and illustrated in Fig. 14(a). In the second stage in Fig. 11(c), the leaf $u_{\Gamma,3}$ is further expanded with respect to the branch of type Fig. 12(e). This expansion process is illustrated in Fig. 14(b). The external momentum variables for $u_{\Gamma,3}(\mathbf{p}')$ are given by $\mathbf{p}' = (p'_1, p'_2, p'_3, p'_4) = (1-5-6, 2, 3, -1-2-3)$. The functional derivative with respect to the momentum variable $(p'_5, p'_6) = (-p_5, -p_6)$ does not act directly on the branch grown after the leaf with the functional derivative $u_{\Gamma,3}$, but it acts on a branch grown from a consecutive leaf. If the functional derivative would act on the branch grown from the functional derivative leaf, represented by the box, it would yield a second-order functional derivative. However, from Fig. 11(c), we see that it acts on the branch grown from the leaf without functional derivative. Therefore we obtain an expression with two first order functional derivatives, which is diagrammatically depicted in Fig. 14(b). The functional derivative with respect to $G(p_{10}, p_{12})$ originates from $u_{\Gamma,1}$, i.e., from the current branch type, whereas the derivative with respect to $G(p'_5, p'_6)$ originates from $u_{\Gamma,3}$. We consider the extended momentum conservation rule (C19). The analytic expression corresponding to this expansion step is given by

$$\begin{aligned} \sum_{5, \dots, 13} K^{(4)}(1, 5, \dots, 13) \frac{\delta u_{\Gamma,1}(-8, -11, -13, -9)}{G_{5',6'}} & \\ \times \frac{\delta u_{\Gamma,1}(-7, 2', 3', 4')}{\delta G_{10,12}} & \end{aligned}$$

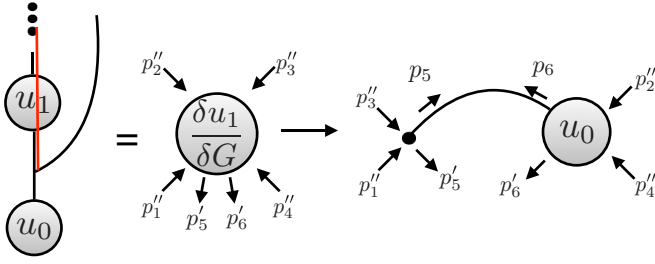


FIG. 15. A functional derivative is acting on a branch. In this stage of the tree expansion, the grown branch corresponds to the second line in (C4). Therefore the functional derivative can act on one of the two G lines, which is equivalent to cutting out one of them. The momentum carried by the functional derivative is assigned to the open ends produced in that way.

$$\begin{aligned}
 &= G_{1'-5,-6,7} G_{10,11} G_{12,13} G_{5,8} G_{6,9} \frac{\delta u_{\Gamma,1}(-7, 2', 3', 4')}{\delta G_{10,12}} \\
 &\quad \times \frac{\delta u_{\Gamma,1}(-8, -11, -13, -9)}{\delta G_{5',6'}} \\
 &\stackrel{G=G_{\text{phys}}}{=} G_{1'-7-8} G_9 G_{1'+2'+3'+4'-7-8-9} G_7 G_8 \\
 &\quad \times \frac{\delta u_{\Gamma,1}(7, 9, 1' + 2' + 3' + 4' - 7 - 8 - 9, 8)}{\delta G_{5',6'}} \\
 &\quad \times \frac{\delta u_{\Gamma,1}(1' - 7 - 8, 2', 3', 4')}{\delta G_{9,1'+2'+3'+4'-7-8-9}}, \quad (\text{C20})
 \end{aligned}$$

where we have established the generalized momentum conservation rule for $p_{12} = p'_1 + p'_2 + p'_3 + p'_4 - p_5 - p_6 - p_{10}$ and renamed in the last equality the integration variables in order to distinguish them from the integration variables of the previous expansion stage. This example shows that even though the functional derivative with respect to $G(5', 6')$ only acts on a branch consecutive to the leaf $u_{\Gamma,1}$ which for itself is not a leaf with a functional derivative the information about the excess momentum running over this leaf has to be stored. Therefore an additional line through the rooted tree is drawn, which indicates that the excess momentum has to be accounted for on the intermediate leaves by using the extended momentum conservation (C19). The excess momentum is removed if the arc line meets the additional line. This additional diagrammatic element is shown as the red line in Figs. 11(b), 11(c), 14(a), and 14(b).

Finally, in the next two expansion stages, the functional derivatives act on the branches. The functional derivative acting on a branch can be graphically depicted as just cutting out one of the two-point correlation function lines. This is shown in Fig. 15 for a particular example. It corresponds to the last expansion stage in Fig. 11(c) where the right leaf $u_{\Gamma,1}$ is expanded. It is assumed that the t -permutation channel is picked. The external momentum of the leaf $u_{\Gamma,1}(\mathbf{p}'')$ is $\mathbf{p}'' = (7, 9, 1' + 2' + 3' + 4' - 7 - 8 - 9, 8)$. The analytic expression for the differentiated branch is given by

$$\begin{aligned}
 &\left(\frac{\delta}{\delta G(5', 6')} G_{5,6} G_{1+3-5,7} \right) u_{\Gamma,0}(-6, -7, 2'', 4'') \\
 &\stackrel{G=G_{\text{phys}}}{=} G_{1''+3''-5''} u_{\Gamma,0}(\mathbf{p}'''). \quad (\text{C21})
 \end{aligned}$$

The new external variable for the leaf grown from the differentiated branch $u_{\Gamma,0}(\mathbf{p}''')$ is $\mathbf{p}''' = (-6', 1'' + 3'' - 10, 2'', 4'')$. Inserting the expression for the primed variables we find that $u_{\Gamma,0}$ is evaluated at $\mathbf{p}''' = (6, -6 - 8 - 9, 9, 8)$. Therefore, after the functional derivative has acted on the branch, the excess momentum is annihilated and momentum conservation at the four-point level is restored.

The discussion of the examples in Fig. 11 provides enough information to write down a set of rules to construct and label all possible rooted trees. A second set of rules assigns to each diagrammatic element in a rooted tree an analytic weight. This makes it possible to design a Monte Carlo algorithm in the space of rooted trees which directly evaluates $\Gamma[G]$ in the subspace of translational invariant G . In the following, we first write down the set of rules to construct and label a random rooted tree. The complete list of diagrammatic elements with their respective weights are tabulated in Appendixes D and E.

We would also like to note that the above examples only discuss the case where the physical subspace is defined by translational invariance. With the same line of arguments it is possible to obtain the construction and evaluation of $\Gamma[G]$ in a physical subspace for general symmetries defined by the collective index space, cf. (B12) and (B33).

The HAM gives a series solution for $\Gamma[G]$, which sums over all deformations $u_{\Gamma,m}$. Thus rooted trees of arbitrary expansion order m have to be considered. The rules to generate a random rooted tree in the tree expansion of an arbitrary $u_{\Gamma,m}$ with external momentum variables \mathbf{p} are. (1) Grow a random branch from the root, i.e., select the expansion of the root into one of the branch types in Fig. 12. For this choice, we assign the labels (k,b,d). The label k stands for the number of leafs grown from the branch, $k=1, 2$. The label $b = \text{bare}$, bold for whether the analytic expression for the branch involves contributions from two-point correlation functions and $d = \text{True}$, False whether one of the leafs is a functional derivative. Thus the respective labeling for the branch types in Fig. 12 are (a) (1,bare,False), (b) (1,bold,False), (c) (2,bold,False), (d) (1,bold,True), and (e) (2,bold,True). The probability to select the chosen (k,b,d) is stored in p_{apriori} in order to obtain the *a priori* probability for the fully grown rooted tree which is needed for the Monte Carlo process. (2) According to the randomly picked branch type add the respective number of leafs with their given type to the tree. If a branch type with $k=2$ was picked one term in the sum $\sum_{i=0}^{m-1}$ has to be chosen randomly, cf. (C4), and the probability for that choice is multiplied to p_{apriori} . If a branch type with $b=\text{bold}$ and $d = \text{False}$ was pick one channel of external leg permutations in the sum \sum_c has to be chosen randomly, cf. (C4), and the probability for that choice is multiplied to p_{apriori} . Depending on the branch type new momentum variables have to be seeded randomly. These are D -dimensional random vectors in the first Brillouin zone. The number of new momentum variables for the possible types are: (a) 0, (b) 1, (c) 2, (d) 2, and (e) 3. The probability for the choice of momentum variables is multiplied to p_{apriori} .

For the branch types (c) and (e), there are two newly grown leafs. For (c), there are two new momentum variables. We assign the left leaf to represent the deformation evaluated at two external momentum variables and the right leaf depending

on only one. We choose the convention that the first of the two momentum variables is assigned to the left leaf whereas the right leaf depends on both variables.

For (e), there are three momentum variables. The leaf with the functional derivative depends only on two of the three randomly seeded momentum variables. We choose the convention that the first two of these variables are assigned to the functional derivative leaf and the right leaf depends on all three variables.

(3) For each of the new leafs, $u_{\Gamma,m'}$, if $m' > 0$ consider this leaf as a new root and go to 2. If $m' = 0$, a new branch can not be grown.

(4) Start a search through the fully grown rooted tree. For each functional derivative encountered, choose randomly a branch consecutive to the functional derivative leaf. This branch will be differentiated by the functional derivative and therefore the additional bookkeeping line is established. The probability for each choice is multiplied to $p_{a\text{ priori}}$.

(5) Start a search through the fully grown rooted tree. If a differentiated branch is encountered pick randomly a term in the respective list of differentiated kernel functions, cf. Appendix E. Correspondingly, reduce the number of momentum variables of the differentiated branch. The probability for each choice is multiplied to $p_{a\text{ priori}}$.

(6) Start a search through the fully grown rooted tree. For each expansion stage, determine the new external momentum variables of the leafs grown in this expansion stage. This is done with respect to the extended momentum conservation rule (C19), cf. also Appendixes D and E.

(7) Start a search through the fully grown rooted tree. As the momentum variables are now correctly assigned the complete weight of the rooted tree can be determined by multiplying the contributions from the kernel functions and from $u_{\Gamma,0}$ at each expansion into a variable w_{tree} .

Therefore, after having applied the above rules, a randomly grown rooted tree is obtained with a corresponding weight w_{tree} . Together with the *a priori* generation probability $p_{a\text{ priori}}$ this is sufficient to perform a direct sampling of the tree expansion by the rules of detailed balance. Therefore we obtain a stochastic summation of the HAM series solution for the functional integro-differential equation defining $\Gamma[G]$.

We find it convenient to extend the direct sampling of diagram topologies with a Markov chain sampling of the integration variables. For that, we randomly pick a single integration variable of a rooted tree and suggest to update this integration variable by adding a random shift in that momentum variable. After the integration variable has been changed, we start from step 2 in the above set of rules to generate a new weight for the tree with the new integration variable. Together with detailed balance, this is used to

perform a Markov chain sampling of the integration variables. In order to achieve good acceptance ratios for the direct sampling of rooted tree topologies, we restrict the randomly seeded integration variables in each stage of the tree expansion to belong to a small region around zero momentum. Therefore we rely on the Markov chain sampling of integration variables to obtain the integration over the complete first Brillouin zone. This leads to sampling problems for higher deformation orders because the sampling can get stuck in a random rooted tree topology. A Markov chain Monte Carlo algorithm has to be used, which also samples diagram topologies and not only integration variables. Therefore a better starting point to include the functional derivatives, compared to randomly suggesting a rooted tree, is the algorithm developed in Ref. [17].

APPENDIX D: KERNEL FUNCTIONS

In this section, we list the analytic expressions for the different branch types and the new external momentum variables for the corresponding leafs grown from these branches. The analytic expressions give directly the projection into the physical subspace of translational invariant G . We denote the external momentum variables at the leaf from which the branch is grown as $\mathbf{p} = (p_1, p_2, p_3, p_4)$ and assume that this leaf corresponds to a deformation $u_{\Gamma,m}$. We again use the shorthand notation $p_i = i$ and $p_i + p_j = i + j$ and implicitly assume summation over repeated indices.

Figure 12 lists all possible branch types where each branch type accounts for a single line in (C4). Furthermore, we consider functional derivatives in intermediate stages which directly act on the leafs and which have to be accounted for by the momentum conservation rule (C19). These additional functional derivatives are highlighted by the momentum labels l_i . Diagrammatically the branch types are depicted in Fig. 16. The analytic expressions for the different branch types, including the intermediate functional derivatives, are given by (a) the analytic expression for the branch type in Fig. 12(a):

(i) $m \neq 1$,

$$(1 - c_0) \frac{\delta^p u_{\Gamma,m-1}(1, 2, 3, 4)}{\delta G(l_0, l_1) \dots \delta G(l_{2p-2}, l_{2p-1})}, \quad (\text{D1})$$

(ii) $m = 1$,

$$-c_0(u_0(1, 2, 3, 4) - \lambda). \quad (\text{D2})$$

In this case, by definition, there are no intermediate functional derivatives, which directly act on the leaf because $\frac{\delta u_{\Gamma,0}}{\delta G} = 0$.

(2) The analytic expression for the branch type in Fig. 12(b): (i) $c = s$,

$$K_{c=s}^{(1)}(\mathbf{p}_{c=s}, 5, 6, 7) = G(1 + 2 - 5, 7)G(5, 6). \quad (\text{D3})$$

Therefore, at $G(1, 2) = G(1)\delta_{1,-2}$,

$$\sum_{5,6,7} K_{c=s}^{(1)}(\mathbf{p}_{c=s}, 5, 6, 7) \frac{\delta^p u_{\Gamma,m-1}(-7, -6, \mathbf{p}_{\bar{c}=\bar{s}})}{\delta G(l_0, l_1) \dots \delta G(l_{2p-2}, l_{2p-1})} \stackrel{G=G_{\text{phys}}}{=} \sum_5 G(5)G(1+2-5) \frac{\delta^p u_{\Gamma,m-1}(1+2-5, 5, 3, 4)}{\delta G(l_0, l_1) \dots \delta G(l_{2p-2}, l_{2p-1})}. \quad (\text{D4})$$

(ii) $c = t, 2 \leftrightarrow 3$; (iii) $c = u, 2 \leftrightarrow 4$.

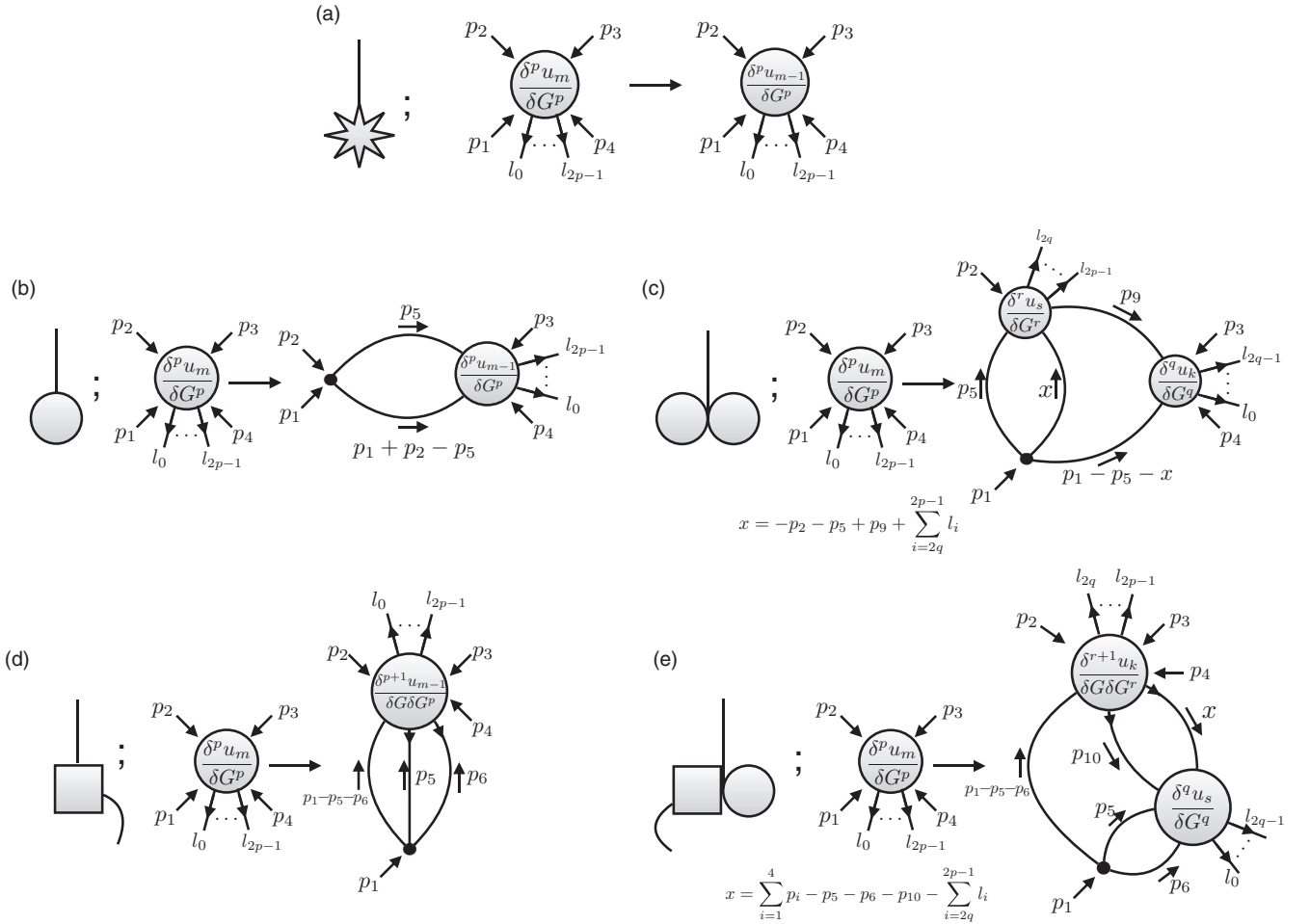


FIG. 16. The diagrammatic expressions for the kernel functions corresponding to each branch type in Fig. 12 in the presence of p intermediate derivatives. In the diagrammatic expressions, the lines correspond to two-point correlation functions with momentum labeled by the arrow. The analytic expression for the contributing kernel function for each branch type can be read off by standard diagrammatic rules. The new external momentum at the newly grown leaves can also be read off by standard diagrammatic rules and taking the extended momentum conservation (C19) rule into account as explained in the main text. The dot represents a bare vertex and therefore ordinary momentum conservation at the four-point level holds there. The momentum variables for the p intermediate derivatives are indicated by l , i.e., $G(l_{2i}, l_{2i+1})$ with $i \in \{0, \dots, p-1\}$. These intermediate derivatives are diagrammatically depicted as the additional lines with arrows on the lines. These arrows indicate that the respective momentum on that line has to be taken into account with an additional minus sign in the extended momentum conservation rule. (a) The branch corresponds to the expansion with respect to the first line in (C4). It contributes with a trivial factor to the rooted tree expansion and does not introduce new integration variables. Therefore the external momentum variables stay the same and the deformation order is reduced from m to $m-1$. (b) The branch corresponds to the expansion with respect to the second line in (C4) and an external leg permutation has to be chosen. In this example, the s channel is chosen. Due to the momentum conservation at the bare vertex the internal momentum variables for the two-point correlation functions are independent of the momentum variables contributing from the intermediate derivatives. (c) The branch corresponds to the expansion with respect to the third line in (C4) and an external leg permutation has to be chosen. In this example, the s channel is chosen. For that branch type, the internal lines depend on the momentum variables of the intermediate derivatives. The convention is picked such that the extended momentum conservation is taken at u_s . In this case, there are two newly grown leaves which can be expanded further and therefore the p intermediate derivatives are distributed randomly such that $r+q=p$. (d) The branch corresponds to the expansion with respect to the fourth line in (C4) and contributes an additional functional derivative. (e) The branch corresponds to the expansion with respect to the fourth line in (C4) and contributes an additional functional derivative on the leaf connected to three external lines. For that branch type, the internal lines depend on the momentum variables of the intermediate derivatives. The convention is picked such that the extended momentum conservation is taken at u_k . In this case, there are two newly grown leaves which can be expanded further and therefore the p intermediate derivatives are distributed randomly such that $r+q=p$.

(c) The analytic expression for the branch type in Fig. 12(c): (i) $c = s$,

$$K_{c=s}^{(2)}(\mathbf{p}_{c=s}, 5, \dots, 11) = G(1-5-7, 11)G(5, 6)G(7, 8)G(9, 10). \quad (\text{D5})$$

Therefore, at $G(1, 2) = G(1)\delta_{1,-2}$ and taking into account the extended momentum conservation (C19) at $u_{\Gamma,k}$,

$$\sum_{5,\dots,11} K_{c=s}^{(2)}(\mathbf{p}_{c=s}, 5, \dots, 11) \frac{\delta^r u_{\Gamma,s}(-6, -8, p_{c=s}, -9)}{\delta G(l_{2q}, l_{2q+1}) \dots \delta G(l_{2p-2}, l_{2p-1})} \frac{\delta^q u_{\Gamma,k}(-11, -10, \mathbf{p}_{\bar{c}=\bar{s}})}{\delta G(l_0, l_1) \dots \delta G(l_{2q-2}, l_{2q-1})}$$

$$\stackrel{G=G_{\text{phys}}}{=} \sum_{5,9} G(5)G(9)G(x)G(1-5-x) \frac{\delta^r u_{\Gamma,s}(5, 2, -9, x)}{\delta G(l_{2q}, l_{2q+1}) \dots \delta G(l_{2p-2}, l_{2p-1})} \frac{\delta^q u_{\Gamma,k}(1-5-x, 9, 3, 4)}{\delta G(l_0, l_1) \dots \delta G(l_{2q-2}, l_{2q-1})}, \quad (\text{D6})$$

where

$$x = -p_2 - p_5 + p_9 + \sum_{i=2q}^{2p-1} l_i. \quad (\text{D7})$$

(ii) $c = t, 2 \leftrightarrow 3$; (iii) $c = u, 2 \leftrightarrow 4$; where $s = m - 1 - k$ with $k \in \{0, \dots, m - 1\}$ and $r + q = p$ with $q \in \{0, \dots, p\}$.

(d) The analytic expression for the branch type in Fig. 12(d):

$$K^{(3)}(1, 5, \dots, 9) = G(1-5-6, 7)G(5, 8)G(6, 9). \quad (\text{D8})$$

Therefore, evaluating the kernel function at $G(1, 2) = G(1)\delta_{1,-2}$,

$$\sum_{5,\dots,9} K^{(3)}(1, 5, \dots, 9) \frac{\delta^{p+1} u_{\Gamma,m-1}(-7, 2, 3, 4)}{\delta G(8, 9)\delta G(l_0, l_1) \dots G(l_{2p-2}, l_{2p-1})}$$

$$\stackrel{G=G_{\text{phys}}}{=} \sum_{5,6} G(1-5-6)G(5)G(6) \frac{\delta^{p+1} u_{\Gamma,m-1}(1-5-6, 2, 3, 4)}{\delta G(-5, -6)\delta G(l_0, l_1) \dots G(l_{2p-2}, l_{2p-1})}. \quad (\text{D9})$$

(e) The analytic expression for the branch type in Fig. 12(e):

$$K^{(4)}(1, 5, \dots, 13) = G(1-5-6, 7)G(5, 8)G(6, 9)G(10, 11)G(12, 13). \quad (\text{D10})$$

Therefore, evaluating the kernel function at $G(1, 2) = G(1)\delta_{1,-2}$,

$$\sum_{5,\dots,13} K^{(4)}(1, 5, \dots, 13) \frac{\delta^{r+1} u_{\Gamma,k}(-7, 2, 3, 4)}{\delta G(10, 12)\delta G(l_{2q}, l_{2q+1}) \dots G(l_{2p-2}, l_{2p-1})} \frac{\delta^q u_{\Gamma,s}(-8, -11, -13, -9)}{\delta G(l_0, l_1) \dots G(l_{2q-2}, l_{2q-1})}$$

$$\stackrel{G=G_{\text{phys}}}{=} \sum_{5,6,10} G(1-5-6)G(5)G(6)G(10)G(x) \frac{\delta^{r+1} u_{\Gamma,k}(1-5-6, 2, 3, 4)}{\delta G(10, x)\delta G(l_{2q}, l_{2q+1}) \dots G(l_{2p-2}, l_{2p-1})} \frac{\delta^q u_{\Gamma,s}(5, 10, x, 6)}{\delta G(l_0, l_1) \dots G(l_{2q-2}, l_{2q-1})}, \quad (\text{D11})$$

where

$$x = \sum_{i=1}^4 p_i - p_5 - p_6 - p_{10} - \sum_{i=2q}^{2p-1} l_i, \quad (\text{D12})$$

and $s = m - 1 - k$ with $k \in \{0, \dots, m - 1\}$, $r + q = p$ with $q \in \{0, \dots, p\}$.

APPENDIX E: FUNCTIONAL DERIVATIVES OF KERNEL FUNCTIONS

In this section, we list the analytic expressions for the functional derivative of the different branch types and the resulting new external momentum variables for the corresponding leafs grown from these differentiated branches in the presence of intermediate functional derivatives. The momentum variables of the functional derivative differentiating the considered branch are denoted by l_0, l_1 if there is a single derivative acting on the branch and l_0, \dots, l_3 if there are two derivatives. Further p intermediate derivatives are labeled with consecutive numbers l_2, \dots, l_{2p+1} and l_4, \dots, l_{2p+3} , respectively. During the Monte Carlo run we measure the average number of functional derivatives. We find that this number is around unity for the parameter range considered in Fig. 3 and the maximal expansion order $m = 6$ reached in our Monte Carlo algorithm. Therefore we list here the kernel functions up to second order derivatives for the branch types Figs. 12(b) and 12(c), which contribute itself no functional derivative and up to first order for the branch types Figs. 12(d) and 12(e), which contribute itself a functional derivative to the rooted tree. We note that we do not restrict the maximal number of functional derivative in a rooted tree but only the number of derivative, which can act on a single branch. Bookkeeping of higher order derivatives of the kernel function, i.e., up to a maximum of 5 for Fig. 12(e) will become increasingly difficult.

The analytic expressions for the derivatives of the various branches are the following. (a) This branch contributes with a trivial factor and therefore can not be differentiated, i.e., the derivative on that branch yields a zero contribution.

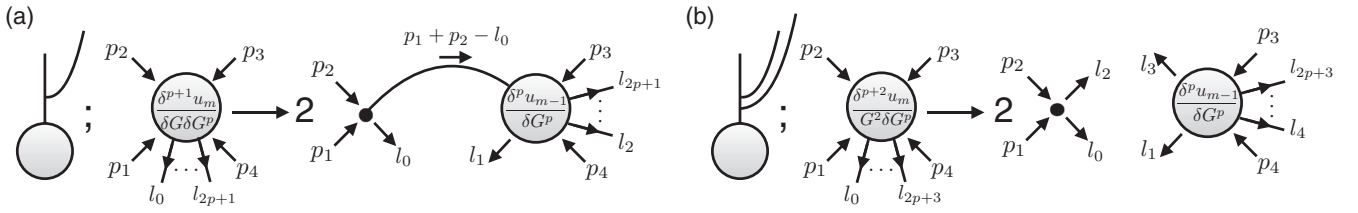


FIG. 17. The first and second functional derivatives of the branch Fig. 12(b) with respect to $G(l_0, l_1)$ and $G(l_0, l_1)G(l_2, l_3)$, respectively. Whereas the first derivative eliminates the integration variable of the differentiated branch, the second derivative contributes a delta function. Therefore the integration variable of the branch on which l_0 or l_2 depends has to be changed such that the delta constrain is satisfied. Alternatively, the integration variable of the branch on which l_1 or l_3 depends can be changed such that the extended momentum conservation rule (C19) is satisfied at the new leaf. In this case also the constrain by the delta function is met automatically.

(b) The diagrammatic expression for the first and second derivative are shown in Fig. 17.

(1) (i) $c = s$,

$$\sum_{5,6,7} \left(\frac{\delta}{\delta G(l_0, l_1)} K_{c=s}^{(1)}(\mathbf{p}_{c=s}, 5, 6, 7) \right) \frac{\delta^p u_{\Gamma, m-1}(-7, -6, \mathbf{p}_{\bar{c}=\bar{s}})}{\delta G(l_2, l_3) \dots \delta G(l_{2p}, l_{2p+1})} \stackrel{G=G_{\text{phys}}}{=} 2G(1+2-l_0) \frac{\delta^p u_{m-1}(-l_1, 1+2-l_0, 3, 4)}{\delta G(l_2, l_3) \dots \delta G(l_{2p}, l_{2p+1})}. \quad (\text{E1})$$

(ii) $c = t, 2 \leftrightarrow 3$. (iii) $c = u, 2 \leftrightarrow 4$.

(2) (i) $c = s$,

$$\sum_{5,6,7} \left(\frac{\delta}{\delta G(l_0, l_1) \delta G(l_2, l_3)} K_{c=s}^{(1)}(\mathbf{p}_{c=s}, 5, 6, 7) \right) \frac{\delta^p u_{\Gamma, m-1}(-7, -6, \mathbf{p}_{\bar{c}=\bar{s}})}{\delta G(l_4, l_5) \dots \delta G(l_{2p+1}, l_{2p+3})} \stackrel{G=G_{\text{phys}}}{=} 2\delta(1+2-l_0-l_2) \frac{\delta^p u_{\Gamma, m-1}(-l_1, -l_3, 3, 4)}{\delta G(l_4, l_5) \dots \delta G(l_{2p+1}, l_{2p+3})}. \quad (\text{E2})$$

(ii) $c = t, 2 \leftrightarrow 3$. (iii) $c = u, 2 \leftrightarrow 4$.

(c) The diagrammatic expressions for the first and second derivative are shown in Figs. 18 and 19. Due to the product rule, the differentiation of the branch yields 4 possible terms where 2 are symmetric to each other. A random rooted tree corresponds to the random choice of a single term.

(1) (i) $c = s$,

$$\begin{aligned} & \sum_{5, \dots, 11} \left(\frac{\delta}{\delta G(l_0, l_1)} K_{c=s}^{(2)}(\mathbf{p}_{c=s}, 5, \dots, 11) \right) \frac{\delta^r u_{\Gamma, s}(-6, p_{c=s}, -9, -8)}{\delta G(l_{2q+2}, l_{2q+3}) \dots \delta G(l_{2p}, l_{2p+1})} \frac{\delta^q u_{\Gamma, k}(-11, -10, \mathbf{p}_{\bar{c}=\bar{s}})}{\delta G(l_2, l_3) \dots \delta G(l_{2q}, l_{2q+1})} \\ & \stackrel{G=G_{\text{phys}}}{=} \sum_5 G(5)G(x)G(1-l_0-x) \frac{\delta^r u_{\Gamma, s}(-l_1, 2, -5, 1-l_0-x)}{\delta G(l_{2q+2}, l_{2q+3}) \dots \delta G(l_{2p}, l_{2p+1})} \frac{\delta^q u_{\Gamma, k}(x, 5, 3, 4)}{\delta G(l_2, l_3) \dots \delta G(l_{2q}, l_{2q+1})} \\ & + \sum_5 G(5)G(y)G(\alpha) \frac{\delta^r u_{\Gamma, s}(5, 2, -\alpha, y)}{\delta G(l_{2q+2}, l_{2q+3}) \dots \delta G(l_{2p}, l_{2p+1})} \frac{\delta^q u_{\Gamma, k}(l_1, \alpha, 3, 4)}{\delta G(l_2, l_3) \dots \delta G(l_{2q}, l_{2q+1})} \\ & + \sum_5 G(5)G(z)G(1-5-z) \frac{\delta^r u_{\Gamma, s}(-l_1, 2, -5, 1-l_0-x)}{\delta G(l_{2q+2}, l_{2q+3}) \dots \delta G(l_{2p}, l_{2p+1})} \frac{\delta^q u_{\Gamma, k}(x, 5, 3, 4)}{\delta G(l_2, l_3) \dots \delta G(l_{2q}, l_{2q+1})}, \quad (\text{E3}) \end{aligned}$$

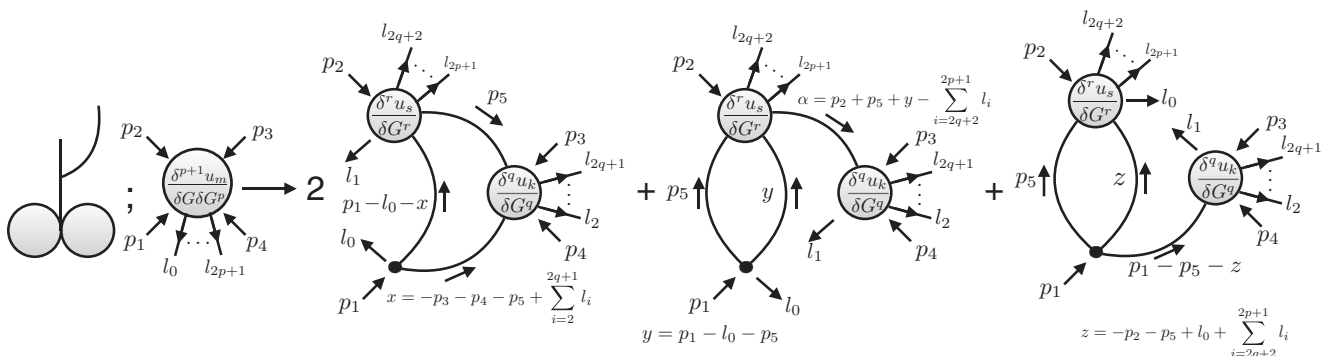


FIG. 18. The first functional derivative of the branch Fig. 12(c) with respect to $G(l_0, l_1)$. Due to the product rule of functional derivatives the differentiation of the branch yields four terms. As two of the terms are symmetric to each other three distinct terms are generated.

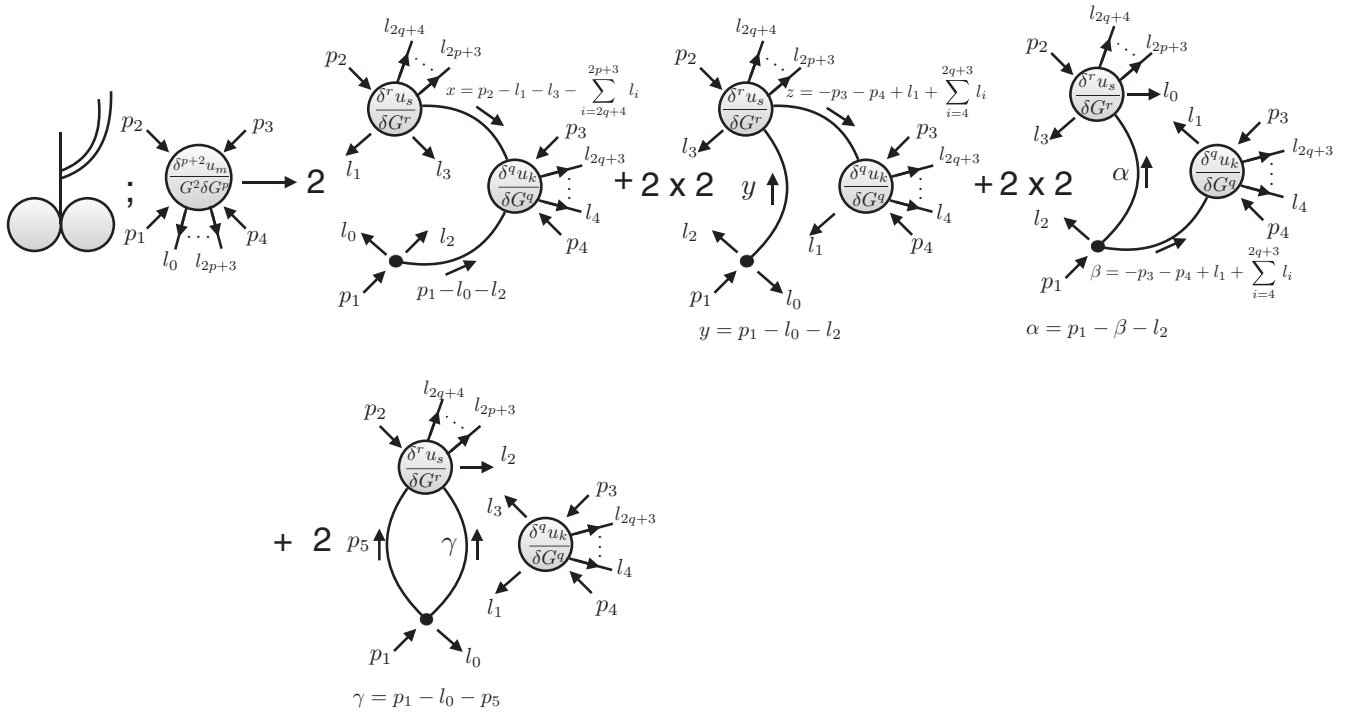


FIG. 19. The second functional derivative of the branch Fig. 12(c) with respect to $G(l_0, l_1)G(l_2, l_3)$. Due to the product rule of functional derivatives the differentiation of the branch yields 12 terms. Due to symmetry considerations there are only four distinct terms. Additional factors of 2 in the least three terms are due to the fact that second-order derivatives commute.

where

$$x = -p_3 - p_4 - p_5 + \sum_{i=2}^{2q+1} l_i, \quad y = p_1 - l_0 - p_5, \quad z = -p_4 - p_5 + l_0 + \sum_{i=2q+2}^{2p+1} l_i, \quad \alpha = p_2 + p_5 + y - \sum_{i=2q+2}^{2p+1} l_i. \quad (\text{E4})$$

(ii) $c = t$, $2 \leftrightarrow 3$. (iii) $c = u$, $2 \leftrightarrow 4$, where $s = m - 1 - k$ with $k \in \{0, \dots, m - 1\}$ and $r + q = p$ with $q \in \{0, \dots, p\}$.

(2) (i) $c = s$,

$$\begin{aligned} & \sum_{5, \dots, 11} \left(\frac{\delta}{\delta G(l_0, l_1) \delta G(l_2, l_3)} K_{c=s}^{(2)}(\mathbf{p}_{c=s}, 5, \dots, 11) \right) \frac{\delta^r u_{\Gamma, s}(-6, p_{c=s}, -9, -8)}{\delta G(l_{2q+4}, l_{2q+5}) \dots \delta G(l_{2p+2}, l_{2p+3})} \frac{\delta^q u_{\Gamma, k}(-11, -10, \mathbf{p}_{\bar{c}=\bar{s}})}{\delta G(l_4, l_5) \dots \delta G(l_{2q+2}, l_{2q+3})} \\ & \stackrel{G=G_{\text{phys}}}{=} 2G(1 - l_0 - l_2)G(x) \frac{\delta^r u_{\Gamma, s}(-l_1, 2, -x, p_1 - l_0 - x)}{\delta G(l_{2q+4}, l_{2q+5}) \dots \delta G(l_{2p+2}, l_{2p+3})} \frac{\delta^q u_{\Gamma, k}(1 - l_0 - l_2, x, 3, 4)}{\delta G(l_4, l_5) \dots \delta G(l_{2q+2}, l_{2q+3})} \\ & + 4G(y)G(z) \frac{\delta^r u_{\Gamma, s}(-l_3, 2, -z, y)}{\delta G(l_{2q+4}, l_{2q+5}) \dots \delta G(l_{2p+2}, l_{2p+3})} \frac{\delta^q u_{\Gamma, k}(-l_1, z, 3, 4)}{\delta G(l_4, l_5) \dots \delta G(l_{2q+2}, l_{2q+3})} \\ & + 4G(\alpha)G(\beta) \frac{\delta^r u_{\Gamma, s}(-l_3, 2, -l_0, \alpha)}{\delta G(l_{2q+4}, l_{2q+5}) \dots \delta G(l_{2p+2}, l_{2p+3})} \frac{\delta^q u_{\Gamma, k}(\beta, -l_1, 3, 4)}{\delta G(l_4, l_5) \dots \delta G(l_{2q+2}, l_{2q+3})} \\ & + 2 \sum_5 G(5)G(\gamma) \frac{\delta^r u_{\Gamma, s}(5, 2, -l_2, \gamma)}{\delta G(l_{2q+4}, l_{2q+5}) \dots \delta G(l_{2p+2}, l_{2p+3})} \frac{\delta^q u_{\Gamma, k}(-l_1, -l_3, 3, 4)}{\delta G(l_4, l_5) \dots \delta G(l_{2q+2}, l_{2q+3})} \delta \left(p_3 + p_4 - l_1 - l_3 - \sum_{i=4}^{2q+3} l_i \right), \end{aligned} \quad (\text{E5})$$

where

$$\begin{aligned} x &= p_2 - l_1 - l_3 - \sum_{i=2q+4}^{2p+3} l_i, \quad y = p_1 - l_0 - l_2, \quad z = -p_3 - p_4 + l_1 + \sum_{i=4}^{2q+3} l_i, \quad \alpha = p_1 - \beta - l_2, \\ \beta &= -p_3 - p_4 + l_1 + \sum_{i=4}^{2q+3} l_i, \quad \gamma = p_1 - l_0 - p_5. \end{aligned} \quad (\text{E6})$$

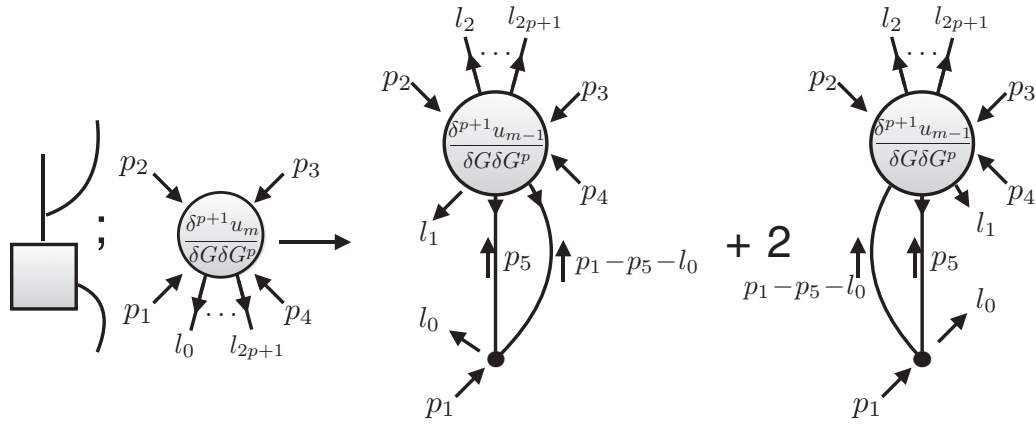


FIG. 20. The first functional derivative of the branch Fig. 12(d) with respect to $G(l_0, l_1)$. This branch type contributes itself a further functional derivative.

(ii) $c = t, 2 \leftrightarrow 3$. (iii) $c = u, 2 \leftrightarrow 4$, where $s = m - 1 - k$ with $k \in \{0, \dots, m - 1\}$ and $r + q = p$ with $q \in \{0, \dots, p\}$.

(d) The diagrammatic expression for the first derivative is shown in Fig. 20.

(1)

$$\sum_{5, \dots, 9} \left(\frac{\delta}{\delta G(l_0, l_1)} K^{(3)}(1, 5, \dots, 9) \right) \frac{\delta^{p+1} u_{\Gamma, m-1}(-7, 2, 3, 4)}{\delta G(8, 9) \delta G(l_2, l_3) \dots G(l_{2p}, l_{2p+1})}$$

$$\stackrel{G=G_{\text{phys}}}{=} \sum_5 G(5) G(1 - 5 - l_0) \frac{\delta^{p+1} u_{m-1}(l_1, 2, 3, 4)}{\delta G(-5, -1 + 5 + l_0) \delta G(l_2, l_3) \dots G(l_{2p}, l_{2p+1})}$$

$$+ 2 \sum_5 G(5) G(1 - 5 - l_0) \frac{\delta^{p+1} u_{m-1}(1 - 5 - l_0, 2, 3, 4)}{\delta G(-5, l_1) \delta G(l_2, l_3) \dots G(l_{2p}, l_{2p+1})}. \tag{E7}$$

(e) The diagrammatic expression for the first derivative is shown in Fig. 21.

(1)

$$\sum_{5, \dots, 13} \left(\frac{\delta}{\delta G(l_0, l_1)} K^{(4)}(1, 5, \dots, 13) \right) \frac{\delta^q u_{\Gamma, s}(-8, -11, -13, -9)}{\delta G(l_2, l_3) \dots G(l_{2q}, l_{2q+1})} \frac{\delta^{r+1} u_{\Gamma, k}(-7, 2, 3, 4)}{\delta G(10, 12) \delta G(l_{2q+2}, l_{2q+3}) \dots G(l_{2p}, l_{2p+1})}$$

$$\stackrel{G=G_{\text{phys}}}{=} \sum_{5, 7} G(5) G(7) G(1 - 5 - l_0) G(x) \frac{\delta^q u_{\Gamma, s}(5, 7, x, 1 - 5 - l_0)}{\delta G(l_2, l_3) \dots G(l_{2p}, l_{2p+1})} \frac{\delta^{r+1} u_{\Gamma, k}(-l_1, 2, 3, 4)}{\delta G(7, x) \delta G(l_{2q+2}, l_{2q+3}) \dots G(l_{2p}, l_{2p+1})}$$

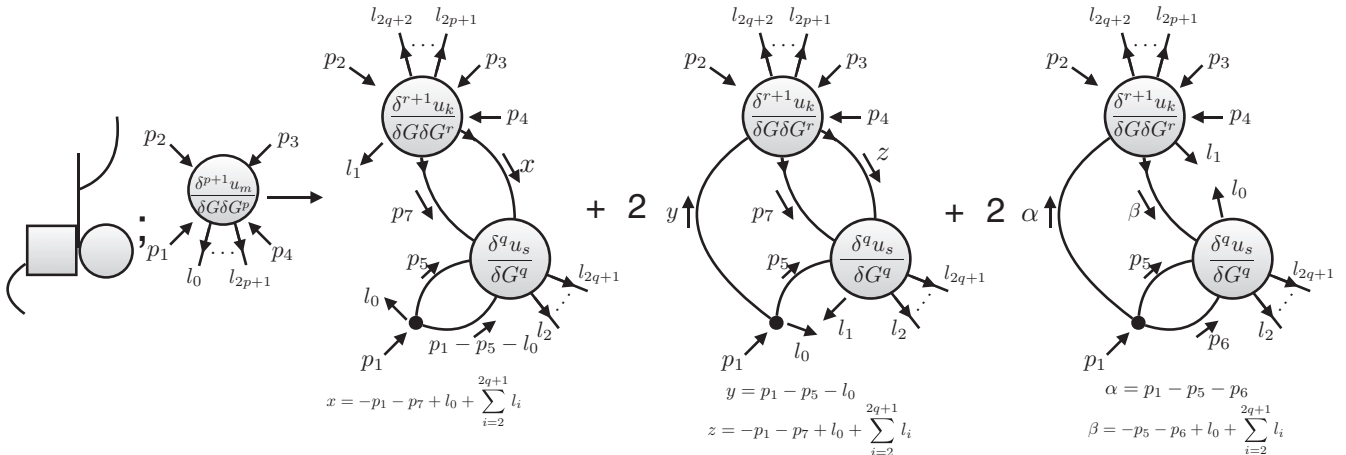


FIG. 21. The first functional derivative of the branch Fig. 12(e) with respect to $G(l_0, l_1)$. This branch type contributes itself a further functional derivative.

$$\begin{aligned}
& + 2 \sum_{5,7} G(5)G(7)G(y)G(z) \frac{\delta^q u_{\Gamma,s}(5, 7, z, -l_1)}{\delta G(l_2, l_3) \dots G(l_{2p}, l_{2p+1})} \frac{\delta^{r+1} u_{\Gamma,k}(y, 2, 3, 4)}{\delta G(7, z) \delta G(l_{2q+2}, l_{2q+3}) \dots G(l_{2p}, l_{2p+1})} \\
& + 2 \sum_{5,6} G(5)G(6)G(\alpha)G(\beta) \frac{\delta^q u_{\Gamma,s}(5, \beta, -l_0, 6)}{\delta G(l_2, l_3) \dots G(l_{2p}, l_{2p+1})} \frac{\delta^{r+1} u_{\Gamma,k}(y, 2, 3, 4)}{\delta G(\beta, l_1) \delta G(l_{2q+2}, l_{2q+3}) \dots G(l_{2p}, l_{2p+1})}, \tag{E8}
\end{aligned}$$

where

$$\begin{aligned}
x &= -p_1 - p_7 + l_0 + \sum_{i=2}^{2q+1} l_i, & y &= p_1 - p_5 - l_0, & z &= -p_1 - p_7 + l_0 + \sum_{i=2}^{2q+1} l_i, \\
\alpha &= p_1 - p_5 - p_6, & \beta &= -p_5 - p_6 + l_0 + \sum_{i=2}^{2q+1} l_i, \tag{E9}
\end{aligned}$$

where $s = m - 1 - k$ with $k \in \{0, \dots, m - 1\}$ and $r + q = p$ with $q \in \{0, \dots, p\}$.

-
- [1] L. Pollet, *Rep. Prog. Phys.* **75**, 094501 (2012).
[2] O. F. Syljuåsen and A. W. Sandvik, *Phys. Rev. E* **66**, 046701 (2002).
[3] R. Blankenbecler, D. J. Scalapino, and R. L. Sugar, *Phys. Rev. D* **24**, 2278 (1981).
[4] A. N. Rubtsov, V. V. Savkin, and A. I. Lichtenstein, *Phys. Rev. B* **72**, 035122 (2005).
[5] E. Gull, A. J. Millis, A. I. Lichtenstein, A. N. Rubtsov, M. Troyer, and P. Werner, *Rev. Mod. Phys.* **83**, 349 (2011).
[6] M. Troyer and U.-J. Wiese, *Phys. Rev. Lett.* **94**, 170201 (2005).
[7] N. V. Prokof'ev and B. V. Svistunov, *Phys. Rev. Lett.* **81**, 2514 (1998).
[8] N. Prokof'ev and B. Svistunov, *Phys. Rev. B* **77**, 020408(R) (2008).
[9] J. Greitemann and L. Pollet, *SciPost Phys. Lect. Notes* **2** (2018).
[10] R. Rossi, *Europhys. Lett.* **118**, 10004 (2017).
[11] J. Vlietinck, J. Ryckebusch, and K. Van Houcke, *Phys. Rev. B* **89**, 085119 (2014).
[12] P. Kroiss and L. Pollet, *Phys. Rev. B* **90**, 104510 (2014).
[13] W. Wu, M. Ferrero, A. Georges, and E. Kozik, *Phys. Rev. B* **96**, 041105(R) (2017).
[14] R. Rossi, *Phys. Rev. Lett.* **119**, 045701 (2017).
[15] G. Cohen, E. Gull, D. R. Reichman, and A. J. Millis, *Phys. Rev. Lett.* **115**, 266802 (2015).
[16] R. E. V. Profumo, C. Groth, L. Messio, O. Parcollet, and X. Waintal, *Phys. Rev. B* **91**, 245154 (2015).
[17] T. Pfeffer and L. Pollet, *New J. Phys.* **19**, 043005 (2017).
[18] N. Prokof'ev and B. Svistunov, *Phys. Rev. Lett.* **99**, 250201 (2007).
[19] S. J. Liao, *Homotopy Analysis Method in Nonlinear Differential Equations* (Springer and Higher Education Press, Berlin, Beijing, 2012).
[20] K. Vajravelu and R. A. Van Gorder, *Nonlinear Flow Phenomena and Homotopy Analysis* (Springer and Higher Education Press, Heidelberg, Beijing, 2012).
[21] P. V. Buividovich, *Nucl. Phys. B* **853**, 688 (2011).
[22] P. V. Buividovich and A. Davody, *Phys. Rev. D* **96**, 114512 (2017).
[23] M. Q. Huber, D. R. Campagnari, and H. Reinhardt, *Phys. Rev. D* **91**, 025014 (2015).
[24] M. Q. Huber, *Phys. Rev. D* **93**, 085033 (2016).
[25] R. Alkofera and L. von Smekal, *Phys. Rep.* **353**, 281 (2001).
[26] L. Hedin, *Phys. Rev. A* **139**, A796 (1965).
[27] C. de Dominicis and P. C. Martin, *J. Math. Phys.* **5**, 14 (1964).
[28] J. Berges, N. Tetradis, and C. Wetterich, *Phys. Rep.* **363**, 223 (2002).
[29] W. Metzner, M. Salmhofer, C. Honerkamp, V. Meden, and K. Schönhammer, *Rev. Mod. Phys.* **84**, 299 (2012).
[30] L. Pollet, N. V. Prokof'ev, and B. V. Svistunov, *Phys. Rev. Lett.* **105**, 210601 (2010).
[31] R. J. Rivers, *Path Integral Methods in Quantum Field Theories* (Cambridge University Press, Cambridge, 1990).
[32] E. Hille, *Ordinary Differential Equations in the Complex Domain* (Wiley & Sons, New York, 1976).
[33] I. R. C. Buckley, A. Duncan, and H. F. Jones, *Phys. Rev. D* **47**, 2554 (1993).
[34] H. Kleinert, *Path Integrals in Quantum Mechanics, Statistics, Polymer Physics, and Financial Markets* (World Scientific, Singapore, 2004).
[35] R. Rossi, F. Werner, N. V. Prokof'ev, and B. V. Svistunov, *Phys. Rev. B* **93**, 161102(R) (2016).
[36] M. Serone, G. Spada, and G. Villadoro, *J. High Energy Phys.* **05** (2017) 056.
[37] L. Pollet, M. N. Kiselev, N. V. Prokof'ev, and B. V. Svistunov, *New J. Phys.* **18**, 113025 (2016).
[38] N. Prokof'ev and B. Svistunov, *Phys. Rev. Lett.* **87**, 160601 (2001).
[39] <https://gitlab.lrz.de/QSIMCORR/DysonSchwingerEquations>.
[40] J. K. Freericks and V. Zlatić, *Rev. Mod. Phys.* **75**, 1333 (2003).